*Inorg. Chem.* **2004**, *43*, 2355–2367


# Mononuclear and Dinuclear Complexes of Dibenzoeilatin: Synthesis, Structure, and Electrochemical and Photophysical Properties

**Sheba D. Bergman,[†] Israel Goldberg,[†] Andrea Barbieri,[‡] Francesco Barigelletti,*[,‡] and Moshe Kol*[,†]**

*The School of Chemistry, Raymond and Beverly Sackler Faculty of Exact Sciences, Tel Aviv University, Tel Aviv 69978, Israel, and Istituto ISOF-CNR, Via P. Gobetti 101, 40129 Bologna, Italy*

Received December 7, 2003

This work describes a study of Ru(II) and Os(II) polypyridyl complexes of the symmetrical, fused-aromatic bridging ligand dibenzoeilatin (**1**). The synthesis, purification, and structural characterization by NMR of the mononuclear complexes $[Ru(bpy)_2(dbneil)]^{2+}$ (**2**), $[Ru(tmbpy)_2(dbneil)]^{2+}$ (**3**), and $[Os(bpy)_2(dbneil)]^{2+}$ (**4**), the homodinuclear complexes $[\{Ru(bpy)_2\}_2\{\mu\text{-dbneil}\}]^{4+}$ (**5**), $[\{Ru(tmbpy)_2\}_2\{\mu\text{-dbneil}\}]^{4+}$ (**6**), and $[\{Os(bpy)_2\}_2\{\mu\text{-dbneil}\}]^{4+}$ (**7**), and the heterodinuclear complex $[\{Ru(bpy)_2\}\{\mu\text{-dbneil}\}\{Os(bpy)_2\}]^{4+}$ (**8**) are described, along with the crystal structures of **4**, **6**, and **7**. Absorption spectra of the mononuclear complexes feature a low-lying MLCT band around 600 nm. The coordination of a second metal fragment results in a dramatic red shift of the MLCT band to beyond 700 nm. Cyclic and square wave voltammograms of the mononuclear complexes exhibit one reversible metal-based oxidation, as well as several ligand-based reduction waves. The first two reductions, attributed to reduction of the dibenzoeilatin ligand, are substantially anodically shifted compared to $[M(bpy)_3]^{2+}$ (M = Ru, Os), consistent with the low-lying $\pi^*$ orbital of dibenzoeilatin. The dinuclear complexes exhibit two reversible, well-resolved, metal-centered oxidation waves, despite the chemical equivalence of the two metal centers, indicating a significant metal–metal interaction mediated by the conjugated dibenzoeilatin ligand. Luminescence spectra, quantum yield, and lifetime measurements at room temperature in argon-purged acetonitrile have shown that the complexes exhibit $^3$MLCT emission, which occurs in the IR-region between 950 and 1300 nm. The heterodinuclear complex **8** exhibits luminescence only from the Ru-based fragment, the intensity of which is less than 1% of that observed in the corresponding homodinuclear complex **5**; no emission from the Os-based unit is observed, and an intramolecular quenching constant of $k_q \geq 3 \times 10^9\ s^{-1}$ is evaluated. The nature of the quenching process is briefly discussed.

## Introduction

There has been considerable interest in Ru(II) and Os(II) polypyridyl complexes because they possess a unique combination of chemical stability and interesting electrochemical and photophysical properties.[1] Such complexes have been employed as sensitizing dyes in the conversion of solar energy to electrical energy,[2] as photo- and redox-active units in various molecular machines and devices,[3] and as photoprobes for nucleic acids.[4] The properties of such complexes can be tuned by judicious choice of the ligands that bind to the metal center. Extended fused aromatic ligands

* To whom correspondence should be addressed. E-mail: moshekol@post.tau.ac.il (M.K.); franz@isof.cnr.it (F.B.).
[†] Tel Aviv University.
[‡] Istituto ISOF-CNR.

(1) (a) Juris, A.; Balzani, V.; Barigelletti, F.; Campagna, S.; Belser, P.; Von Zelewsky, A. *Coord. Chem. Rev.* **1988**, *84*, 85. (b) Balzani, V.; Scandola, F. *Supramolecular Photochemistry*; Ellis Horwood: Chichester, U.K., 1991. (c) Sauvage, J.-P.; Collin, J.-P.; Chambron, J.-C.; Guillerez, S.; Coudret, C.; Balzani, V.; Barigelletti, F.; De Cola, L.; Flamigni, L. *Chem. Rev.* **1994**, *94*, 993. (d) Balzani, V.; Juris, A.; Venturi, M.; Campagna, S.; Serroni, S. *Chem. Rev.* **1996**, *96*, 759.

(2) (a) Kalyanasundaram, K.; Grätzel, M. *Coord. Chem. Rev.* **1998**, *77*, 347. (b) Bignozzi, C. A.; Argazzi, R.; Kleverlaan, C. J. *Chem. Soc. Rev.* **2000**, *29*, 87. (c) Kelly, C. A.; Meyer, G. J. *Coord. Chem. Rev.* **2001**, *211*, 295. (d) Anderson, P. A.; Keene, F. R.; Meyer, T. J.; Moss, J. A.; Strouse, G. F.; Treadway, J. A. *J. Chem. Soc., Dalton Trans.* **2002**, 3820.

(3) (a) Belser, P.; Bernhard, S.; Blum, C.; Beyeler, A.; De Cola, L.; Balzani, V. *Coord. Chem. Rev.* **1999**, *190*−*192*, 155. (b) Ballardini, R.; Balzani, V.; Credi, A.; Gandolfi, M. T.; Venturi, M. *Acc. Chem. Res.* **2001**, *34*, 445. (c) Ashton, P. R.; Ballardini, R.; Balzani, V.; Credi, A.; Dress, K. R.; Ishow, E.; Kleverlaan, C. J.; Kocian, O.; Preece, J. A.; Spencer, N.; Stoddart, J. F.; Venturi, M.; Wenger, S. *Chem. Eur. J.* **2000**, *6*, 3558. (d) Ashton, P. R.; Ballardini, R.; Balzani, V.; Constable, E. C.; Credi, A.; Kocian, O.; Langford, S. J.; Preece, J. A.; Prodi, L.; Schofield, E. R.; Spencer, N.; Stoddart, J. F.; Wenger, S. *Chem. Eur. J.* **1998**, *4*, 2413.

10.1021/ic0354062 CCC: $27.50 
Published on Web 02/26/2004

have attracted much attention due to their potential use as nucleic acid intercalators,[5] and as mediators of energy and electron transfer.[6] Such ligands bearing more than one coordination site are of particular interest because they can be used as bridging ligands in polynuclear assemblies. The fused aromatic system renders the ligand rigidity, a fixed distance and orientation between the coordination sites, and, due to the delocalized nature of such ligands, usually permits greater electronic communication between the metal centers via the superexchange mechanism.[7]

Thus far, a wide variety of fused aromatic bridging ligands have been introduced, the majority of which possess 2,2′-bipyridine- (bpy) or 1,10-phenanthroline- (phen) type coordination sites (e.g., tpphz[8] and its analogues,[9] HAT,[10] and ppz[11]). Bridging ligands bearing 2,2′-biquinoline- (biq) type coordination sites are less common.[12] In addition, to the best of our knowledge, there are no reports in the literature of a fully fused-aromatic bridging ligand that is not planar.[13]

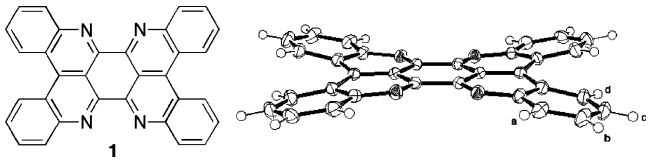


**1**

**Figure 1.** Molecular and X-ray structure of the symmetrical bridging ligand dibenzoeilatin (**1**). The curvature of **1** stems from steric interactions between the protons in the "bay" region ($H^d$).[14]

Dibenzoeilatin (**1**) is a synthetic compound composed of nine fused-aromatic rings arranged in a highly symmetric manner, leading to two identical biq-type coordination sites. Compound **1** is not planar due to steric interactions between protons in the "bay" region, termed the $H^d$ protons; instead, it has a curved surface reminiscent of an S shape (Figure 1). In a recent preliminary study, we have reported that the mononuclear dibenzoeilatin complex $[Ru(bpy)_2(dbneil)][PF_6]_2$ (**2**) (dbneil = dibenzoeilatin) exhibits several unique features:[14] a tilted binding of the dibenzoeilatin ligand which results from steric interactions with the protons of the bpy ligands; formation of tight discrete dimers in solution held together by complementary $\pi-\pi$ stacking interactions via the dibenzoeilatin moiety;[15] and a low-lying metal-to-ligand charge-transfer (MLCT) absorption band, having a $\lambda_{max}$ of 594 nm. In the present study we set forth to explore the potential of this unique compound as a bridging ligand and gain insight on the properties of its resulting dinuclear complexes. Specifically, we wished to address the following topics: the tendency to form dinuclear complexes and their diastereoisomeric preference; the degree of communication between the two metal centers bridged by this nonplanar conjugated ligand; the effect of binding a second metal fragment on the low-lying MLCT band; and the nature of the excited state. We thus report the synthesis, NMR characterization, crystal structures, electrochemical behavior, and photophysical properties (from absorption and near-IR emission results) of the new mononuclear complexes $[Ru(bpy)_2(dbneil)]^{2+}$ (**2**), $[Ru(tmbpy)_2(dbneil)]^{2+}$ (**3**), and $[Os(bpy)_2(dbneil)]^{2+}$ (**4**), the homodinuclear complexes $[\{Ru(bpy)_2\}_2\{\mu\text{-dbneil}\}]^{4+}$ (**5**), $[\{Ru(tmbpy)_2\}_2\{\mu\text{-dbneil}\}]^{4+}$ (**6**), and $[\{Os(bpy)_2\}_2\{\mu\text{-dbneil}\}]^{4+}$ (**7**), and the heterodinuclear complex $[\{Ru(bpy)_2\}\{\mu\text{-dbneil}\}\{Os(bpy)_2\}]^{4+}$ (**8**).


(4) (a) Van Gijte, O.; Kirsch-De Mesmaeker, A. *J. Chem. Soc., Dalton Trans.* **1999**, 951. (b) Foley, F. M.; Keene, F. R.; Collins, J. G. *J. Chem. Soc., Dalton Trans.* **2001**, 2968. (c) Wilhelmsson, L. M.; Westerlund, F.; Lincoln, P.; Nordén, B. *J. Am. Chem. Soc.* **2002**, *124*, 12092. (d) Patterson, B. T.; Collins, J. G.; Foley, F. M.; Keene, F. R. *J. Chem. Soc., Dalton Trans.* **2002**, 4343. (e) Kirsch-De Mesmaeker, A.; Moucheron, C.; Boutonnet, N. *J. Phys. Org. Chem.* **1998**, *11*, 566.

(5) (a) Erkkila, K. E.; Odom, D. T.; Barton, J. K. *Chem. Rev.* **1999**, *99*, 2777. (b) Dupureur, C. M.; Barton, J. K. *Inorg. Chem.* **1997**, *36*, 33. (c) Holmlin, R. E.; Yao, J. A.; Barton, J. K. *Inorg. Chem.* **1999**, *38*, 174. (d) Gregurić, A.; Gregurić, I. D.; Hambley, T. W.; Aldrich-Wright, J. R.; Collins, J. G. *J. Chem. Soc., Dalton Trans.* **2002**, 849. (e) Morgan, R. J.; Chatterjee, S.; Baker, A. D.; Strekas, T. C. *Inorg. Chem.* **1991**, *30*, 2687. (f) Brodkorb, A.; Kirsch-De Mesmaeker, A.; Rutherford, T. J.; Keene, F. R. *Eur. J. Inorg. Chem.* **2001**, 2151.

(6) See for example: (a) Chiorboli, C.; Rodgers, M. A. J.; Scandola, F. *J. Am. Chem. Soc.* **2003**, *125*, 483. (b) Kim, M.-J.; Konduri, R.; Ye, H.; MacDonnell, F. M.; Puntoriero, F.; Serroni, S.; Campagna, S.; Holder, T.; Kinsel, G.; Rajeshwar, K. *Inorg. Chem.* **2002**, *41*, 2471. (c) Campagna, S.; Serroni, S.; Bodige, S.; MacDonnell, F. M. *Inorg. Chem.* **1999**, *38*, 692. (d) Konduri, R.; Ye, H.; MacDonnell, F. M.; Serroni, S.; Campagna, S.; Rajeshwar, K. *Angew. Chem., Int. Ed.* **2002**, *41*, 3185.

(7) (a) MacConnell, H. M. *J. Chem. Phys.* **1961**, *35*, 508. (b) Newton, M. D. *Chem. Rev.* **1991**, *91*, 767. (c) Giuffrida, G.; Campagna, S. *Coord. Chem. Rev.* **1994**, *135/136*, 517.

(8) See for example: (a) Bolger, J.; Gourdon, A.; Ishow, E.; Launay, J.-P. *J. Chem. Soc., Chem. Commun.* **1995**, 1799. (b) Bolger, J.; Gourdon, A.; Ishow, E.; Launay, J.-P. *Inorg. Chem.* **1996**, *35*, 2937. (c) Bodige, S.; Torres, A. S.; Maloney, D. J.; Tate, D.; Kinsel, G. R.; Walker, A. K.; MacDonnell, F. M. *J. Am. Chem. Soc.* **1997**, *119*, 10364. (d) Chiorboli, C.; Bignozzi, C. A.; Scandola, F.; Ishow, E.; Gourdon, A.; Launay, J.-P. *Inorg. Chem.* **1999**, *38*, 2402. (e) Campagna, S.; Serroni, S.; Bodige, S.; MacDonnell, F. M. *Inorg. Chem.* **1999**, *38*, 692. (f) Kim, M.-J.; MacDonnell, F. M.; Gimon-Kinsel, M. E.; Du Bois, T.; Asgharian, N.; Griener, J. C. *Angew. Chem., Int. Ed.* **2000**, *39*, 615.

(9) See for example: (a) Komatsuzaki, N.; Katoh, R.; Himeda, Y.; Sugihara, H.; Arakawa, H.; Kasuga, K. *J. Chem. Soc., Dalton Trans.* **2000**, 3053. (b) Ishow, E.; Gourdon, A.; Launay, J.-P. *Chem. Commun.* **1998**, 1909. (c) Ishow, E.; Gourdon, A.; Launay, J.-P.; Chiorboli, C.; Scandola, F. *Inorg. Chem.* **1999**, *38*, 1504. (d) Wärnmark, K.; Heyke, O.; Thomas, J. A.; Lehn, J.-M. *Chem. Commun.* **1996**, 2603. (e) MacDonnell, F. M.; Kim, M.-J.; Wouters, K. L.; Konduri, R. *Coord. Chem. Rev.* **2003**, *242*, 47 and references therein.

(10) See for example: (a) Masschelein, A.; Kirsch-De Mesmaeker, A.; Verhoeven, C.; Nasielski-Hinkens, R. *Inorg. Chim. Acta* **1987**, *129*, L13. (b) Rutherford, T. J.; Keene, F. R. *Inorg. Chem.* **1997**, *36*, 3580. (c) Rutherford, T. J.; Van Gijte, O.; Kirsch-De Mesmaeker, A.; Keene, F. R. *Inorg. Chem.* **1997**, *36*, 4465. (d) Brodkorb, A.; Kirsch-De Mesmaeker, A.; Rutherford, T. J.; Keene, F. R. *Eur. J. Inorg. Chem.* **2001**, 2151. (e) Rutherford, T. J.; Keene, F. R. *J. Chem. Soc., Dalton Trans.* **1998**, 1155. (f) Moucheron, C.; Kirsch-De Mesmaeker, A. *J. Am. Chem. Soc.* **1996**, *118*, 12834.

(11) See for example: (a) Fuchs, Y.; Lofters, S.; Dieter, T.; Shi, W.; Morgan, R.; Strekas, T. C.; Gafney, H. D.; Baker, A. D. *J. Am. Chem. Soc.* **1987**, *109*, 2691. (b) Morgan, O.; Wang, S.; Bae, S.-A.; Morgan, R. J.; Baker, A. D.; Strekas, T. C.; Engel, R. *J. Chem. Soc., Dalton Trans.* **1997**, 3773.

(12) Diquinoxalino[2,3-a:2′,3′-c]phenazine is a fully fused-aromatic biq-type bridging ligand, but it has not been used as a bridging ligand for Ru(II) and Os(II). It has been used as a bridging ligand for Ag(I); see for example: (a) Bu, X.-H.; Biradha, K.; Yamaguchi, T.; Nishimura, M.; Ito, T.; Tanaka, K.; Shionoya, M. *Chem. Commun.* **2000**, 1953. (b) Kitagawa, S.; Masaoka, S. *Coord. Chem. Rev.* **2003**, *246*, 73. In addition, there are 2-pyrido quinoline-type ligands such as dpop; see for example: (c) Ruminski, R. R.; Serveiss, D.; Jacquez, M. *Inorg. Chem.* **1995**, *34*, 3358. (d) Ruminski, R. R.; Deere, P. T.; Olive, M.; Serveiss, D. *Inorg. Chim. Acta* **1998**, *281*, 1 and references therein.

(13) We define a nonplanar bridging ligand as a ligand that is distorted from planarity prior to coordination of a metal. There are several examples in the literature of bridging ligands that develop distortions upon binding of a metal; see for example: (a) D'Alessandro, D. M.; Kelso, L. S.; Keene, F. R. *Inorg. Chem.* **2001**, *40*, 6841. (b) Reference 34.

(14) Bergman, S. D.; Reshef, D.; Groysman, S.; Goldberg, I.; Kol, M. *Chem. Commun.* **2002**, 2374.

## Experimental Section

**Materials.** Dibenzoeilatin (**1**),[16] tmbpy,[17] *rac,cis*-[Ru(tmbpy)$_2$Cl$_2$],[18] *rac,cis*-[Os(bpy)$_2$Cl$_2$],[19] and *rac*-[Ru(bpy)$_2$(dbneil)][PF$_6$]$_2$ (**2**)[14] were synthesized according to the literature procedures. Tetra-*n*-butylammonium hexafluorophosphate (98%) and silver nitrate (99.995%) were purchased from Aldrich and used without further purification. Acetonitrile for photophysical experiments was of spectroscopic grade. All other chemicals and solvents were of reagent grade and used without further purification, except for acetonitrile for electrochemical measurements, which was distilled over $CaH_2$. All the reactions and electrochemical measurements were performed under an argon atmosphere.

**Instrumentation.** $^1$H and $^{13}$C NMR, COSY, NOESY, and HMQC experiments were performed on a Bruker Avance 400 spectrometer using the residual protons of the solvent ($CD_3CN$) as an internal standard at $\delta = 1.93$ ppm. FABMS data were obtained on a VG-AutoSpec M250 mass spectrometer, in a *m*-nitrobenzyl alcohol matrix. MALDI-TOF MS experiments were performed using a Voyager-DE STR mass spectrometer (Applied Biosystems) in the positive ion reflector mode. The measurements were obtained in a cyano-3-hydroxycinnamic acid matrix, with internal calibration (Applied Biosystems calibration mixture 2). Elemental analyses were performed in the microanalytical laboratory in the Hebrew University of Jerusalem. UV−vis absorption spectra in acetonitrile were obtained on a Kontron UVIKRON 931 UV−vis spectrometer.

Cyclic and square wave voltammograms were carried out on a $\mu$-autolab type II potentiostat (Eco Chemie), using a platinum working electrode, a platinum auxiliary electrode, and a Ag/$AgNO_3$ (0.01 M in acetonitrile) reference electrode (Bioanalytical Systems). The measurements were carried out on the complexes dissolved in argon-purged acetonitrile containing 0.1 M tetra-*n*-butylammonium hexafluorophosphate (TBAH) as supporting electrolyte. The typical concentration of the complexes was ca. 1.5 mM. The criteria for reversibility were the separation between the cathodic and anodic peaks (not exceeding 90 mV), the close-to-unity ratio of the intensities of the cathodic and anodic peak currents, and the constancy of the peak potential on changing scan rate. A 5 mM solution of ferrocene in acetonitrile containing 0.1 M TBAH was measured after the measurement of each complex, typically yielding a value of $E_{1/2} = 0.096$ V for Fc/Fc$^+$. Values were converted to the SCE scale assuming $E_{1/2} = 400$ mV for Fc/Fc$^+$.[20]

The luminescence spectra for ca. $2 \times 10^{-5}$ M argon-purged acetonitirile solutions were measured using an Edinburgh FLS920 spectrometer equipped with a Hamamatsu R5509-72 supercooled photomultiplier tube (193 K), a TM300 emission monochromator with NIR grating blazed at 1000 nm, and an Edinburgh Xe900 450 W xenon arc lamp as light source. An excitation wavelength of 440 nm was used for all complexes, which leads to final population of the lowest-lying luminescent levels of Ru- or Os-based metal-to-ligand charge-transfer nature (see Results section).[21,22] Corrected luminescence spectra in the range 540−1600 nm were obtained by using a correction curve for the phototube response provided by the manufacturer. Luminescence quantum yields ($\Phi$) were evaluated by comparing wavelength-integrated intensities ($I$) with reference to [Ru(bpy)$_3$]Cl$_2$ ($\Phi_r = 0.028$ in air-equilibrated water[23]), [Ru(bpy)$_3$][PF$_6$]$_2$ ($\Phi_r = 0.062$ in argon-purged acetonitrile solution[22]), or [Os(bpy)$_3$][PF$_6$]$_2$ ($\Phi_r = 0.005$ in argon-purged acetonitrile solution[22]) as standards and by using the following equation:[22,24]

$$\frac{\Phi}{\Phi_r} = \frac{A_r n^2 I}{A n_r^2 I_r}$$

where $A$ and $n$ are absorbance values (<0.15) at the employed excitation wavelength and refractive index of the solvent, respectively. Band maxima and relative luminescence intensities are obtained with uncertainty of 2 nm and 20%, respectively. The luminescence lifetimes were obtained with the same equipment operated in single-photon mode by using a 407 nm laser diode excitation controlled by a Hamamatsu C4725 stabilized picosecond light pulser. Analysis of the luminescence decay profiles against time was accomplished by using software provided by the manufacturer. The lifetime values are obtained with an estimated uncertainty of 10%.

**Synthesis. [Ru(tmbpy)$_2$(dbneil)][PF$_6$]$_2$ (3).** *rac,cis*-[Ru(tmbpy)$_2$Cl$_2$] (28.7 mg, 0.048 mmol) and dibenzoeilatin (**1**) (20.0 mg, 0.044 mmol) were added to 6 mL of ethylene glycol and heated to 110 °C for 15 h under an argon atmosphere. The green reaction mixture obtained was cooled to RT, and a sat. $KPF_6$(aq) solution was added until precipitation of a green solid occurred. The solid was isolated by centrifugation and washed several times with water to remove traces of salts. The solid was dried in vacuo and was purified by chromatography on a Sephadex-CM C-25 column using a gradient of NaCl(aq)/$CH_3OH$ = 1:1 as eluent. The mononuclear complex eluted out of the column as an emerald-green band at ionic strength of 0.1−0.15 M NaCl(aq). An additional olive-green band eluted out at higher ionic strength (0.2−0.25 M NaCl(aq)) and was identified as dinuclear complex **6**, yield 29% (14.7 mg). The appropriate fraction was precipitated by addition of a sat $KPF_6$(aq) solution, filtered and dried in vacuo. Compound **3** is obtained as a green solid, in a yield of 62% (34.7 mg). Anal. Calcd (Found) for $C_{60}H_{48}F_{12}N_8P_2Ru\cdot H_2O$: C, 55.86 (55.65); H, 3.91 (3.66); N, 8.68 (8.72). $^1$H NMR ($CD_3CN$, 323 K) $\delta$ 8.725 (d, 2H, $J = 7.4$ Hz, H$^{d}$), 8.649 (d, 2H, $J = 7.0$ Hz, H$^{d'}$), 8.195 (s, 2H, H$^{3'}$), 8.149 (s, 2H, H$^{3}$), 7.741 (t, 2H, $J = 7.8$ Hz, H$^{c}$), 7.60 (m, 8H, H$^{a}$, H$^{b}$, H,[6] H$^{c'}$), 7.51 (m, 4H, H$^{a'}$, H$^{6'}$), 7.446 (t, 2H, $J = 7.0$ Hz, H$^{b'}$), 2.457 (s, 6H, C$H_3^{4'}$), 2.272 (s, 6H, C$H_3^{4}$), 2.14 (s buried under solvent peak, 6H, C$H_3^{5'}$), 1.780 (s, 6H, C$H_3^{5}$). $^{13}$C NMR ($CD_3CN$, 323 K) $\delta$ 154.5 (*C*-H$^{6}$), 151.0 (*C*-H$^{6'}$), 133.0 (*C*-H$^{b'}$), 132.8 (*C*-H$^{a}$), 132.1 (*C*-H$^{b}$), 131.6 (*C*-H$^{c'}$), 130.5 (*C*-H$^{c}$), 129.9 (*C*-H$^{d'}$), 128.3 (*C*-H$^{d}$), 127.0 (*C*-H$^{a'}$), 125.4 (*C*-H$^{3'}$), 125.2 (*C*-H$^{3}$), 19.6 (*C*H$_3^{4'}$), 19.3 (*C*H$_3^{4}$), 16.9 (*C*H$_3^{5'}$), 16.6 (*C*H$_3^{5}$). FABMS: 982.2 [M − 2PF$_6$ + H]$^+$, 1127.2 [M − PF$_6$ + H]$^+$.

**[Os(bpy)$_2$(dbneil)][PF$_6$]$_2$ (4).** This complex was prepared by the same method described for **3**, using *rac,cis*-[Os(bpy)$_2$Cl$_2$] (27.1 mg, 0.047 mmol), dibenzoeilatin (**1**) (18.9 mg, 0.041 mmol), and 8 mL of ethylene glycol, and heating to 120 °C for 24 h. The dark green-brown reaction mixture obtained was processed and purified as described for **3**. Again, the dark brown dinuclear complex **7** was obtained as a byproduct in a yield of 45% (21.7 mg), which was


(15) Gut, D.; Rudi, A.; Kopilov, J.; Goldberg, I.; Kol, M. *J. Am. Chem. Soc.* **2002**, *124*, 5449.
(16) Gellerman, G.; Rudi, A.; Kashman, Y. *Tetrahedron* **1994**, *50*, 12959.
(17) Patterson, B. T.; Keene, F. R. *Inorg. Chem.* **1998**, *37*, 645.
(18) Sullivan, B. P.; Salmon, D. J.; Meyer, T. J. *Inorg. Chem.* **1978**, *17*, 3334.
(19) Kober, E. M.; Caspar, J. V.; Sullivan, B. P.; Meyer, T. J. *Inorg. Chem.* **1988**, *27*, 4587.
(20) Connelly, N. G.; Geiger, W. E. *Chem. Rev.* **1996**, *96*, 877.
(21) (a) Yeh, A. T.; Shank, C. V.; McCusker, J. K. *Science* **2000**, *289*, 935. (b) Darmrauer, N. H.; Cerullo, G.; Yeh, A.; Boussie, T. R.; Shank, C. V.; McCusker, J. K. *Science* **1997**, *275*, 54.
(22) (a) Kober, E. M.; Caspar, J. V.; Lumpkin, R. S.; Meyer, T. J. *J. Phys. Chem.* **1986**, *90*, 3722. (b) Fleming, C. N.; Maxwell, K. A.; DeSimone, J. M.; Meyer, T. J.; Papanikolas, J. M. *J. Am. Chem. Soc.* **2001**, *123*, 10336.
(23) Nakamaru, K. *Bull. Chem. Soc. Jpn.* **1982**, *55*, 2967.
(24) Demas, J. N.; Crosby, G. A. *J. Phys. Chem.* **1971**, *75*, 991.

successfully separated from **4** by ion-exchange chromatography employing the same conditions described for **3**. Compound **4** is obtained as a green solid, in a yield of 50% (26.0 mg). Anal. Calcd (Found) for $C_{52}H_{32}F_{12}N_8OsP_2 \cdot 2H_2O$: C, 48.60 (48.81); H, 2.82 (2.60); N, 8.72 (8.71).$^1$H NMR ($CD_3CN$, 320 K) $\delta$ 8.995 (d, 2H, $J = 7.6$ Hz, $H^d$), 8.977 (d, 2H, $J = 6.9$ Hz, $H^{d'}$), 8.537 (d, 2H, $J = 8.1$ Hz, $H^{3'}$), 8.418 (d, 2H, $J = 8.2$ Hz, $H^3$), 8.242 (broad d, 2H, $H^{a'}$), 7.986 (t, 2H, $J = 8.6$ Hz, $H^{4'}$), 7.966 (t, 2H, $J = 8.1$ Hz, $H^{b'}$), 7.923 (t, 2H, $J = 8.5$ Hz, $H^{c'}$), 7.802 (t, 2H, $J = 7.7$ Hz, $H^4$), 7.763 (t, 2H, $J = 7.5$ Hz, $H^c$), 7.739 (d, 2H, $J = 5.3$ Hz, $H^{6'}$), 7.67 (broad d, 2H, $H^6$), 7.518 (t, 2H, $J = 6.2$ Hz, $H^{5'}$), 7.401 (t, 2H, $J = 7.4$ Hz, $H^b$), 7.11 (m, 4H, H,[5] $H^a$). $^{13}$C NMR ($CD_3CN$, 320 K) $\delta$ 155.6 (*C*-$H^6$), 152.0 (*C*-$H^{6'}$), 140.9 (*C*-$H^{4'}$), 139.6 (*C*-$H^4$), 133.8 (*C*-$H^{b'}$), 133.6 (*C*-$H^b$), 132.6 (*C*-$H^{a'}$), 132.0 (*C*-$H^c$), 130.8 (*C*-$H^{c'}$), 130.1 (*C*-$H^d$), 129.4 (*C*-$H^5$), 129.3 (*C*-$H^{5'}$), 128.8 (*C*-$H^{d'}$), 126.0 (*C*-$H^a$), 125.5 (*C*-$H^3$), 125.4 (*C*-$H^{3'}$). FABMS: 960.2 $[M - 2PF_6 + H]^+$, 1105.2 $[M - PF_6 + H]^+$.

**[{Ru(bpy)$_2$}$_2${$\mu$-dbneil}][PF$_6$]$_4$ (5).** *rac,cis*-$[Ru(bpy)_2Cl_2]\cdot 2H_2O$ (42.8 mg, 0.082 mmol) and dibenzoeilatin (**1**) (15.0 mg, 0.033 mmol) were added to 8 mL of ethylene glycol and heated to 140 °C for 3 days under an argon atmosphere. The reddish-brown reaction mixture obtained was cooled to RT, and sat. $KPF_6$(aq) solution was added until precipitation of an olive-green solid occurred. The solid was isolated by centrifugation and washed several times with water to remove traces of salts. The solid was dried in vacuo and was purified by recrystallization from $CH_3CN$/ether. The desired complex was obtained as an olive-green solid, yield 97% (59.3 mg). Anal. Calcd (Found) for $C_{72}H_{48}F_{24}N_{12}P_4Ru_2 \cdot 3H_2O$: C, 45.10 (44.86); H, 2.84 (2.57); N, 8.77 (8.60). $^1$H NMR ($CD_3CN$, 298 K, 400 MHz) $\delta$ 9.118 (d, 4H, $J = 8.5$ Hz, $H^d$), 8.535 (d, 4H, $J = 8.1$ Hz, $H^3$), 8.480 (d, 4H, $J = 8.2$ Hz, $H^{3'}$), 8.148 (t, 4H, $J = 7.9$ Hz, $H^4$), 7.98 (m, 8H, $H^c$, $H^{4'}$), 7.900 (m, 4H, $H^6$), 7.708 (d, 4H, $J = 5.5$ Hz, $H^{6'}$), 7.603 (t, 4H, $J = 7.4$ Hz, $H^b$), 7.52 (m, 8H, H,[5] $H^a$), 7.171 (t, 4H, $J = 5.8$ Hz, 1.4 Hz, $H^{5'}$). $^{13}$C NMR ($CD_3CN$, 298 K, 400 MHz) $\delta$ 154.9 (*C*-$H^{6'}$), 152.6 (*C*-$H^6$), 140.5 (*C*-$H^4$), 139.6 (*C*-$H^{4'}$), 134.1 (*C*-$H^b$), 132.5 (*C*-$H^c$), 131.1 (*C*-$H^d$), 129.2 (*C*-$H^5$), 129.2 (*C*-$H^{5'}$), 126.1 (*C*-$H^a$), 125.9 (*C*-$H^{3'}$), 125.8 (*C*-$H^3$). FAB-MS, 1429.3 $[M - 3PF_6 + 2H]^+$, 1574.2 $[M - 2PF_6 + 2H]^+$, 1719.2 $[M - PF_6 + H]^+$.

**[{Ru(tmbp)$_2$}$_2${$\mu$-dbneil}][PF$_6$]$_4$ (6).** This complex was prepared and purified by the same method described for **5**, using *rac,cis*-$[Ru(tmbp)_2Cl_2]$ (49.0 mg, 0.082 mmol) and dibenzoeilatin (**1**) (15.0 mg, 0.033 mmol). The desired complex was obtained as an olive-green solid, yield 96% (65.6 mg). Anal. Calcd (Found) for $C_{88}H_{80}F_{24}N_{12}P_4Ru_2 \cdot H_2O$: C, 50.20 (55.10); H, 3.93 (3.80); N, 7.98 (7.79). FAB-MS, 1654.0 $[M - 3PF_6 + 3H]^+$, 1797.1 $[M - 2PF_6 + H]^+$, 1940.8 $[M - PF_6]^+$. Recrystallization of the complex from $CH_3CN$/ether afforded the separation of the two diastereoisomeric forms of the complex; the *meso* form (28.1 mg) precipitated from the $CH_3CN$/ether solution, whereas the *meso*-contaminated *rac* form (37.5 mg) remained in the mother liquor. The *rac* isomer was eventually purified by repeated crystallizations from the same solvent mixture. Data for *meso*-**6** follow. $^1$H NMR ($CD_3CN$, 298 K, 400 MHz) $\delta$ 9.130 (d, 4H, $J = 8.2$ Hz, $H^d$), 8.261 (s, 4H, $H^3$), 8.171 (s, 4H, $H^{3'}$), 8.979 (broad t, 4H, $H^c$), 7.53 (m, 12H, $H^b$, $H^a$, $H^6$), 7.120 (s, 4H, $H^{6'}$), 2.480 (s, 12H, C$H_3^4$), 2.264 (s, 12H, C$H_3^{4'}$), 2.13 (s buried under solvent signal, 12H, C$H_3^5$), 1.651 (s, 12H, C$H_3^{5'}$). $^{13}$C NMR ($CD_3CN$, 298 K, 400 MHz) $\delta$ 153.8 (*C*-$H^{6'}$), 151.0 (*C*-$H^6$), 133.9 (*C*-$H^b$), 132.1 (*C*-$H^c$), 130.7 (*C*-$H^d$), 126.8 (*C*-$H^a$), 125.7 (*C*-$H^3$), 125.7 (*C*-$H^{3'}$), 19.6 (*C*-$H_3^4$), 19.5 (*C*-$H_3^{4'}$), 17.0 (*C*-$H_3^5$), 16.8 (*C*$H_3^{5'}$). Data for *rac*-**6** follow. $^1$H NMR ($CD_3CN$, 298 K, 400 MHz) $\delta$ 9.132 (broad d, 4H, $H^d$), 8.272 (s, 4H, $H^3$), 8.184 (s, 4H, $H^{3'}$), 8.000 (broad t, 4H, $H^c$), 7.52 (m, 12H, $H^b$, $H^a$, $H^6$), 7.184 (s, 4H, $H^{6'}$), 2.485 (s, 12H, C$H_3^4$), 2.285 (s, 12H, C$H_3^{4'}$), 2.12 (s buried under solvent signal, 12H, C$H_3^5$), 1.626 (s, 12H, C$H_3^{5'}$).

**[{Os(bpy)$_2$}$_2${$\mu$-dbneil}][PF$_6$]$_4$ (7).** This complex was prepared and purified by the same method described for **5**, using *rac,cis*-$[Os(bpy)_2Cl_2]$ (47.1 mg, 0.082 mmol) and dibenzoeilatin (**1**) (15.0 mg, 0.033 mmol), and heating the reaction mixture to 150 °C for 3 days. The desired complex was obtained as a brown solid, yield 84% (57.1 mg). Anal. Calcd (Found) for $C_{72}H_{48}F_{24}N_{12}P_4Os_2 \cdot H_2O$: C, 41.99 (41.77); H, 2.45 (2.50); N, 8.16 (7.92). $^1$H NMR ($CD_3CN$, 298 K, 400 MHz) $\delta$ 9.042 (d, 4H, $J = 8.3$ Hz, $H^d$), 8.596 (d, 4H, $J = 8.1$ Hz, $H^3$), 8.454 (d, 4H, $J = 8.2$ Hz, $H^{3'}$), 8.035 (t, 4H, $J = 8.0$ Hz, $H^4$), 7.932 (t, 4H, $J = 7.5$ Hz, $H^c$), 7.828 (m, 4H, $H^{4'}$), 7.738 (m, 4H, $H^6$), 7.58 (m, 4H, $H^5$), 7.47 (m, 8H, $H^b$, $H^{6'}$), 7.08 (m, 8H, $H^a$, $H^{5'}$). $^{13}$C NMR ($CD_3CN$, 298 K, 400 MHz) $\delta$ 155.1 (*C*-$H^{6'}$), 152.3 (*C*-$H^6$), 141.2 (*C*-$H^4$), 139.7 (*C*-$H^{4'}$), 134.3 (*C*-$H^b$), 132.5 (*C*-$H^c$), 131.1 (*C*-$H^d$), 129.5 (*C*-$H^5$), 129.5 (*C*-$H^{5'}$), 126.3 (*C*-$H^{3'}$), 126.0 (*C*-$H^a$), 125.9 (*C*-$H^3$). FAB-MS, 1607.1 $[M - 3PF_6 + H]^+$, 1574.2 $[M - 2PF_6 + H]^+$, 1719.2 $[M - PF_6 + H]^+$.

**[{(bpy)$_2$Ru}{$\mu$-dbneil}{Os(bpy)$_2$}][PF$_6$]$_4$ (8)** *rac,cis*-$[Os(bpy)_2Cl_2]$ (6.2 mg, 0.011 mmol) and **2** (7.3 mg, 0.006 mmol) were added to 6 mL of ethylene glycol and heated to 140 °C for 3 days under an argon atmosphere. The brown reaction mixture obtained was cooled to RT, and sat. $KPF_6$(aq) solution was added until precipitation of a dark brown solid occurred. The solid was isolated by centrifugation and washed several times with water to remove traces of salts. The solid was dried in vacuo, and then purified by chromatography on a Sephadex LH-20 column using $CH_3CN/CH_3OH = 5{:}1$ as eluent. The appropriate dark brown fraction was collected and the solvent removed in vacuo. The desired complex was obtained as a brown solid, yield 20% (2.4 mg). Alternatively, this complex could be synthesized by reacting **4** (4.8 mg, 0.004 mmol) with *rac,cis*-$[Ru(bpy)_2Cl_2]\cdot 2H_2O$ (2.3 mg, 0.005 mmol) in a similar yield (23%, 1.7 mg). In both cases, homo-bimetallic species did not form, indicating that the mononuclear complexes are coordinatively inert. Anal. Calcd (Found) for $C_{72}H_{48}F_{24}N_{12}P_4OsRu \cdot 2H_2O$: C, 43.49 (43.26); H, 2.64 (2.60); N, 8.45 (8.18). $^1$H NMR ($CD_3CN$, 298 K, 400 MHz) $\delta$ 9.098 (d, 2H, $J = 8.5$ Hz, $H^d$), 9.066 (d, 2H, $J = 8.5$ Hz, $H^{d'}$), 8.602 (d, 2H, $J = 8.1$ Hz, $H^{3''}$), 8.540 (d, 2H, $J = 8.1$ Hz, $H^3$), 8.487 (d, 2H, $J = 8.2$ Hz, $H^{3'}$), 8.451 (d, 2H, $J = 8.2$ Hz, $H^{3'''}$), 8.145 (t, 2H, $J = 7.8$ Hz, $H^4$), 8.045 (t, 2H, $J = 7.9$ Hz, $H^{4''}$), 7.95 (m, 8H, $H^{4'}$, $H^c$, $H^{c'}$, $H^6$), 7.824 (m, 2H, $H^{4'''}$), 7.770 (m, 2H, $H^{6'}$), 7.724 (m, 2H, $H^{6''}$), 7.54 (m, 10H, $H^{5''}$, $H^b$, $H^5$, $H^{b'}$, $H^a$), 7.408 (d, 2H, $J = 5.8$ Hz, $H^{6'''}$), 7.188 (m, 2H, $H^{5'}$), 7.063 (m, 4H, $H^{a'}$, $H^{5'''}$). $^{13}$C NMR ($CD_3CN$, 298 K, 400 MHz) $\delta$ 155.2 (*C*-$H^{6'''}$), 154.9 (*C*-$H^{6'}$), 152.7 (*C*-$H^6$), 152.2 (*C*-$H^{6''}$), 141.4 (*C*-$H^{4''}$), 140.2 (*C*-$H^4$), 139.7 (*C*-$H^{4'''}$), 139.5 (*C*-$H^{4'}$), 134.1 (*C*-$H^b$), 132.5 (*C*-$H^c$), 132.3 (*C*-$H^{c'}$), 131.1 (*C*-$H^{d'}$), 130.8 (*C*-$H^d$), 129.5 (*C*-$H^{5''}$), 129.5 (*C*-$H^{5'''}$), 129.1 (*C*-$H^5$), 129.1 (*C*-$H^{5'}$), 126.3 (*C*-$H^{b'}$), 126.3 (*C*-$H^a$), 126.1 (*C*-$H^{3'}$), 126.1 (*C*-$H^{3'''}$), 126.0 (*C*-$H^{a'}$), 125.9 (*C*-$H^{3''}$), 125.9 (*C*-$H^3$). MALDI-TOF-MS, 1516.2 $[M - 3PF_6]^+$, 1661.2 $[M - 2PF_6]^+$, 1807.2 $[M - PF_6 + H]^+$.

**X-ray Structure Determinations.** The X-ray diffraction measurements were carried out at ca. 110 K on a Nonius Kappa CCD diffractometer, using Mo K$\alpha$ ($\lambda = 0.7101$ Å) radiation. To minimize thermal motion effects and solvent disorder, and to avoid deterioration, the analyzed crystals were embedded within a drop of viscous oil and freeze-cooled to 110 K. Intensity data were corrected for absorption. The crystal structures were solved by Patterson and Fourier techniques (DIRDIF-96)[25] and direct methods (SIR-97),[26] and refined by full-matrix least-squares (SHELXL-97).[27]

**Crystal data for 4.** $C_{66.5}H_{50}F_{12}N_{10}OsP_2$, formula weight 1469.30, triclinic, space group $P\bar{1}$, $a = 13.6830(1)$ Å, $b = 14.1680(1)$ Å, $c = 17.4750(2)$ Å, $\alpha = 79.2050(4)°$, $\beta = 77.5380(4)°$, $\gamma = 63.5320(6)°$, $V = 2945.05(5)$ Å$^3$, $Z = 2$, $D_{calcd} = 1.657$ g·cm$^{-3}$, $F(000) = 1466$, $\mu$(Mo K$\alpha$) = 2.311 mm$^{-1}$, $2\theta_{max} = 59.82°$, 13603 unique reflections were measured. The final refinement converged at R1 = 0.041 and wR2 = 0.099 for 12001 unique observations with [$I > 2\sigma(I)$] and R1 = 0.051 and wR2 = 0.105 for all data. The structure contains partly disordered solvent molecules of toluene located on an inversion center and acetonitrile. Partial rotational disorder characterizes also one of the $PF_6^-$ ions.

**Data for *meso*-6.** $C_{44}H_{62}N_6O_{12}Ru$, formula weight 968.07, triclinic, space group $P\bar{1}$, $a = 11.1240(4)$ Å, $b = 16.0950(7)$ Å, $c = 16.3860(6)$ Å, $\alpha = 61.738(2)°$, $\beta = 87.256(2)°$, $\gamma = 83.989(1)°$, $V = 2569.7(2)$ Å$^3$, $Z = 2$, $D_{calcd} = 1.251$ g·cm$^{-3}$, $F(000) = 1016$, $\mu$(Mo K$\alpha$) = 0.365 mm$^{-1}$, $2\theta_{max} = 51.56°$, 9355 unique reflections were measured. The final refinement converged at R1 = 0.068 and wR2 = 0.171 for 7504 unique observations with [$I > 2\sigma(I)$] and R1 = 0.089 and wR2 = 0.186 for all data. Molecules of the complex are located on centers of inversion. The asymmetric unit of this structure contains, in addition to the two hydroxide counterions, at least 10 molecules of partly disordered molecules of water. The poor quality of the crystals, and thus of the diffraction data, did not allow us to locate reliably all the hydrogen atoms of the located solvent. The final residual electron density map indicates some smeared electron density peaks in void spaces, suggesting the presence of additional solvent species with partial occupancy which were not accounted for in the structural model.

**Data for *meso*-7.** $C_{72}H_{76}Cl_4N_{12}O_{14}Os_2$, formula weight 1855.65, triclinic, space group $P\bar{1}$, $a = 9.6320(2)$ Å, $b = 12.7620(2)$ Å, $c = 16.0470(3)$ Å, $\alpha = 102.0240(7)°$, $\beta = 97.4120(7)°$, $\gamma = 95.678(1)°$, $V = 1896.99(6)$ Å$^3$, $Z = 1$, $D_{calcd} = 1.624$ g·cm$^{-3}$, $F(000) = 924$, $\mu$(Mo K$\alpha$) = 3.557 mm$^{-1}$, $2\theta_{max} = 56.50°$, 8687 unique reflections were measured. The final refinement converged at R1 = 0.036 and wR2 = 0.084 for 7701 unique observations with [$I > 2\sigma(I)$] and R1 = 0.043 and wR2 = 0.088 for all data. There are 14 molecules of water solvent per unit cell. Traces of acetonitrile also seem to be contained in the crystal. One of the chloride anions seems to be disordered between two sites, each of which is occupied in an alternating manner by either $Cl^-$ or a molecule of water. The H-atoms of the water could not be located.

The apparent solvent/anion disorder in **4**, *meso*-**6**, and *meso*-**7** has little effect on the molecular structures of the corresponding dibenzoeilatin complexes.

**NMR Dimerization Experiments.** Typically, a concentrated stock solution (ca. 1 mM) of a complex was prepared by accurately weighing out the dried complex and dissolving it in an accurately measured volume of $CD_3CN$ (4.00−5.00 mL). The concentration dependence of the chemical shifts was studied at constant temperature, measured by the chemical shift of MeOH. Aliquots (50 $\mu$L) of the stock solution were added to an NMR tube initially containing 0.40 mL of $CD_3CN$, and 50 $\mu$L aliquots of $CD_3CN$ were added to an NMR tube initially containing 0.40 mL of the stock solution to obtain a broad concentration range. The NMR spectra were recorded after several minutes of thermal equilibration time, following each addition. The dimerization constants were calculated, based on the chemical shifts of protons $H^d$ and $H^{d'}$, by the method of Horman and Dreux.[28]

**Scheme 1.** Synthesis of Mono- and Dinuclear Complexes of Dibenzoeilatin **2**−**8**

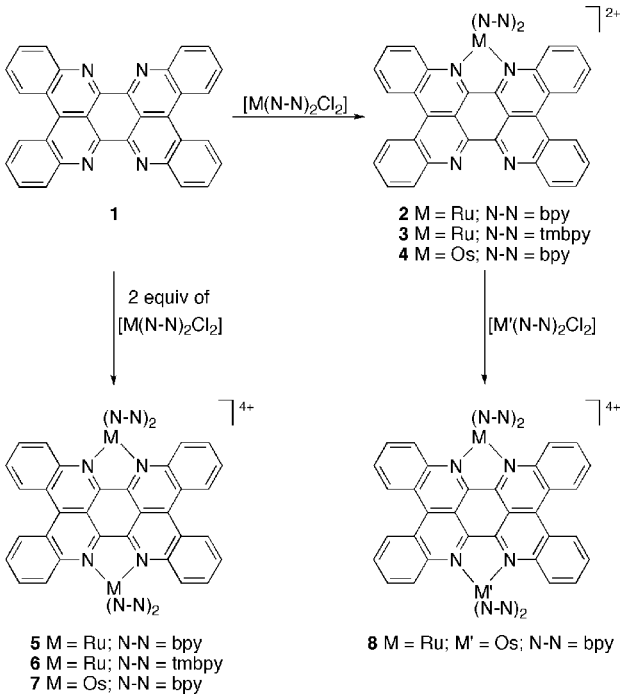


## Results

**Syntheses.** The mononuclear complexes **2**, **3**, and **4** were prepared by reacting dibenzoeilatin with 1−1.1 equiv of the appropriate metal precursor *rac,cis*-[M(N−N)$_2$Cl$_2$] (M = Ru, Os; N−N = bpy, tmbpy) in ethylene glycol, as shown in Scheme 1. The complexes were purified by column chromatography on Sephadex-CM C-25 and isolated as the $PF_6^-$ salts. The homodinuclear complexes were obtained as byproducts in the preparation of the mononuclear counterparts and were also prepared independently (vide infra).

The homodinuclear complexes **5**, **6**, and **7** were prepared by reacting dibenzoeilatin with 2.5 equiv of *rac,cis*-[M(N−N)$_2$Cl$_2$] (M = Ru, Os; N−N = bpy, tmbpy) in ethylene glycol (Scheme 1). The complexes were isolated as the $PF_6^-$ salts and purified by recrystallization from $CH_3CN$/ether. The heterodinuclear complex **8** could be prepared either by reacting **2** with 1.5 equiv of *rac,cis*-[Os(bpy)$_2$Cl$_2$], or by reacting **4** with 1.5 equiv of *rac,cis*-[Ru(bpy)$_2$Cl$_2$]·2H$_2$O. Both routes were evaluated in a low scale (ca. 5 mg) and were found to be equally satisfactory, leading to similar yields of **8**. The higher yields obtained in the synthesis of **2**, compared to **4**, prompted us to use the former as the starting mononuclear dibenzoeilatin complex in the large-scale preparation of **8**. The complex was isolated as the $PF_6^-$ salt and purified by column chromatography on Sephadex LH-20. All complexes were characterized by 1D and 2D NMR techniques, by MS, and by elemental analysis.

(25) Beurskens, P. T.; Beurskens, G.; Bosman, W. P.; de Gelder, R.; Garcia-Granda, S.; Gould, R. O.; Israel, R.; Smits, J. M. M. *DIRDIF-96*; Crystallography Laboratory, University of Nijmegen: Nijmegen, The Netherlands, 1996.

(26) Altomare, A.; Burla, M. C.; Camalli, M.; Cascarano, M.; Giacovazzo, C.; Guagliardi, A.; Polidori, G. SIR-97. *J. Appl. Crystallogr.* **1994**, *27*, 435.

(27) Sheldrick, G. M. *SHELXL-97. Program for the Refinement of Crystal Structures from Diffraction Data*; University of Göttingen: Göttingen, Germany, 1997.

(28) Horman, I.; Dreux, B. *Helv. Chim. Acta* **1984**, *67*, 754.

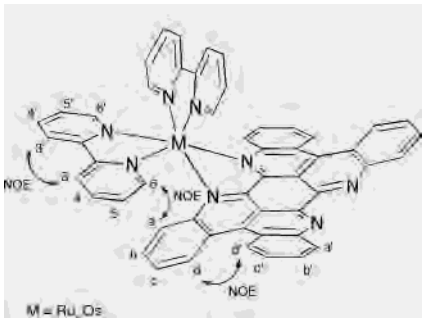


**Figure 2.** Numbering scheme and NOE correlations of the mononuclear complexes **2**, **3**, and **4** (the additional methyl groups in **3** are shown in gray).

Of all the dinuclear complexes, **6** could be separated quantitatively into its two diastereoisomeric forms *meso* ($\Delta\Lambda$) and *rac* ($\Delta\Delta + \Lambda\Lambda$) by recrystallization from $CH_3CN$/ether: The less soluble *meso* isomer (as determined by X-ray analysis, vide infra) precipitated while the *rac* isomer remained in the mother liquor.

**NMR.** The NMR characterization of all the complexes in $CD_3CN$ was achieved by utilization of COSY, NOESY, and HMQC two-dimensional NMR techniques. The $^1$H NMR spectra of all the mononuclear complexes exhibit 8 signals corresponding to the dibenzoeilatin ligand, bound at only one of its two available coordination sites. The spectra are characterized by two closely spaced low-field doublets (appearing at 8.5−8.9 ppm) corresponding to the $H^d$ and $H^{d'}$ protons of the dibenzoeilatin ligand. These protons are located in a "bay" of aromatic rings where they are subjected to ring currents and, therefore, are shifted to lower fields. The metal-bound side of the dibenzoeilatin ligand was identified by a NOE correlation between its $H^a$ protons and the $H^6$ protons of the bpy ligands, as illustrated in Figure 2. As previously described for **2**,[14] the $^1$H NMR chemical shifts of the mononuclear complexes exhibit a strong dependence on concentration and temperature, demonstrated for **4** in Figure 3. This phenomenon is attributed to $\pi-\pi$ stacking of the mononuclear complexes via the dibenzoeilatin moiety. The negligible chemical shift migration exhibited by $H^a$ and $H^b$ further supports their assignment on the metal-bound side, being remote from the effective stacking area.

Octahedral metal centers containing three bidentate ligands are chiral at the metal. The mononuclear dibenzoeilatin complexes having $C_2$-symmetry are obtained as racemic mixtures. The homodinuclear complexes of dibenzoeilatin may exist as two diastereoisomeric forms, i.e., *meso* ($\Delta\Lambda$) and *rac* ($\Delta\Delta + \Lambda\Lambda$). The dinuclear complexes **5** and **7** both exhibit relatively simple $^1$H NMR spectra that seem to indicate the presence of two diastereoisomers as revealed from the broadening and slight splitting of several signals. In contrast, the dinuclear complex **6** clearly exhibits splitting of several of the tmbpy peaks, attributed to the presence of two diastereoisomers (all the other signals coincide). According to the $^1$H NMR specrum of the crude product, these two diastereoisomers (*meso* and *rac*) form as a 1:1 mixture. The two diastereoisomers could be quantitatively separated by recrystallization, and thus, the $^1$H NMR spectra of each diastereoisomeric form could be recorded separately. The *meso* form (as identified by X-ray analysis, vide infra) exhibits higher field signals for the tmbpy protons $H^3$ (8.171 vs 8.184 ppm), $H^6$ (7.120 vs 7.184 ppm), and the protons of the methyl group $CH_3^4$ (2.264 vs 2.285 ppm), compared to the *rac* form. In contrast, the protons of the methyl group $CH_3^5$ exhibit an opposite trend, appearing at a lower field in the *meso* form (1.651 vs 1.626 ppm). Due to the higher symmetry of the homodinuclear complexes relative to their mononuclear counterparts, only four signals appear for the dibenzoeilatin ligand for both the *meso* and *rac* forms, having $C_{2h}$ and $D_2$ symmetries on the NMR time scale, respectively. As observed for the mononuclear complexes, the lowest-field signal (appearing at ca. 9.1 ppm) corresponds to the $H^d$ protons of the dibenzoeilatin ligand. In contrast to their mononuclear counterparts, the $^1$H NMR spectra of the dinuclear complexes are not concentration and temperature dependent. This is rationalized by the incapability of the dinuclear complexes to $\pi$-stack in solution, as the presence of the two bulky $M(N-N)_2$ termini prevents efficient stacking of the dibenzoeilatin moieties.

The $C_2$-symmetric heterodinuclear complex **8** should also form as a mixture of two diastereoisomers. The lower symmetry of **8** is apparent in its $^1$H NMR spectrum, which consists of 24 signals. The spectrum retains the same general features exhibited by the homodinuclear complexes, and it generally appears like a superposition of the spectra of **5** and **7**, with the exception that the peaks are sharper. The assignment of the protons pertaining to a certain metal fragment was accomplished by comparing the spectrum to the spectra of **5** and **7** (Figure 4). It is evident that the Os-bound side of dibenzoeilatin appears at higher fields than the Ru-bound side, as may be explained by stronger back-donation from the metal to the ligand. The formation of **8** as a mixture of two diastereoisomers, i.e., $\Delta\Delta/\Lambda\Lambda$ and $\Delta\Lambda/\Lambda\Delta$, is evident by the splitting of several peaks in the $^1$H NMR spectrum, and their ratio seems to be 1:1 as observed for **6**.

**Structure.** Single crystals of the mononuclear complex **4** suitable for X-ray diffraction were obtained by recrystallization from $CH_3CN$/toluene. A perspective view (ORTEP) of the cation of complex **4** with partial atom numbering is shown in Figure 5 (left), and selected bond distances and angles are given in Table 1. Complex **4** crystallized in a triclinic unit cell of the space group $P\bar{1}$, the asymmetric unit containing one molecule of the complex, two hexafluorophosphate anions, and crystallization solvent (two acetonitrile molecules and four toluene molecules, two of the latter could not be modeled completely). The Os−N bond distances are comparable to those reported for Os−polypyridyl complexes.[29] As observed previously for **2**,[14] the metal fragment of **4** is tilted with respect to the idealized equatorial plane of the $OsN_6$ octahedron, as a result of the steric interactions between the benzo rings of the dibenzoeilatin ligand and the peripheral bpy ligands. The tilt conformation leads to

(29) (a) Shklover, V.; Zakeeruddin, S. M.; Nesper, R.; Fraser, D.; Grätzel, M. *Inorg. Chim. Acta* **1998**, *274*, 64. (b) Richter, M. M.; Scott, B.; Brewer, K. J.; Willett, R. D. *Acta Crystallogr.* **1991**, *C47*, 2443.

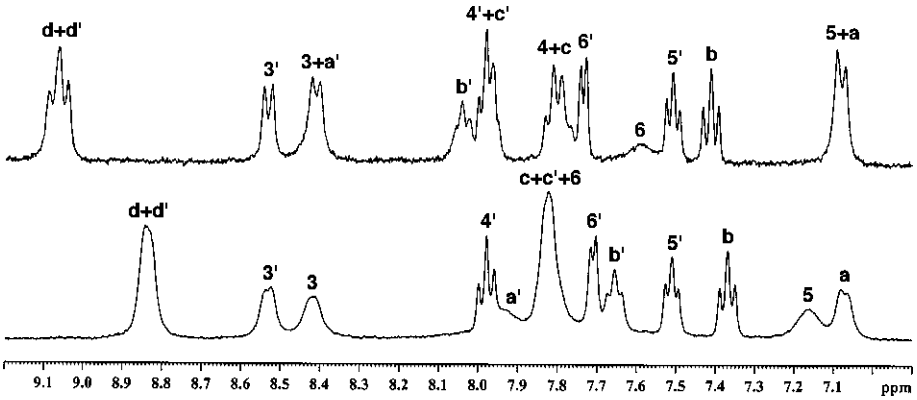


**Figure 3.** Concentration dependence of the $^1$H NMR spectrum of the mononuclear complex **4**. Top: 0.22 mM. Bottom: 0.90 mM.

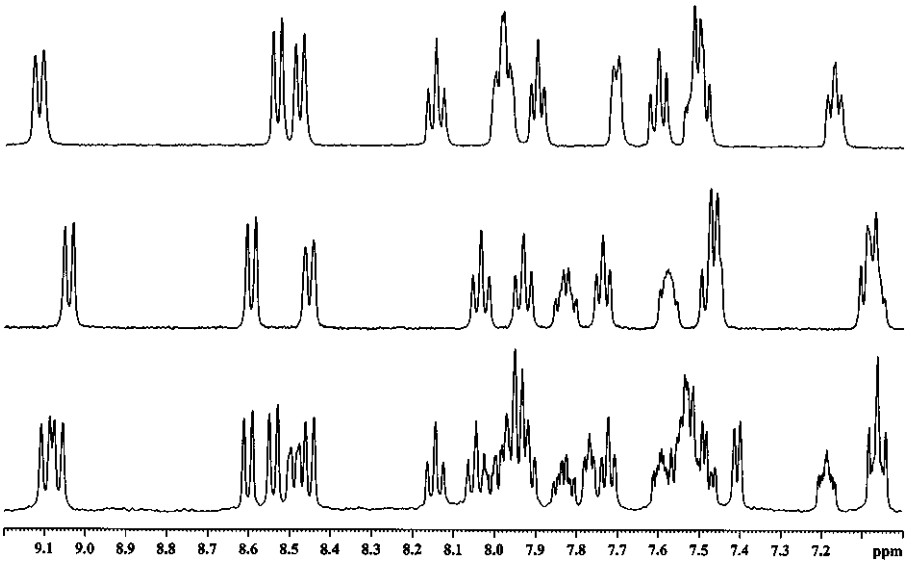


**Figure 4.** $^1$H NMR spectra of the homodinuclear complexes **5** (top) and **7** (middle), and of the heterodinuclear complex **8** (bottom).

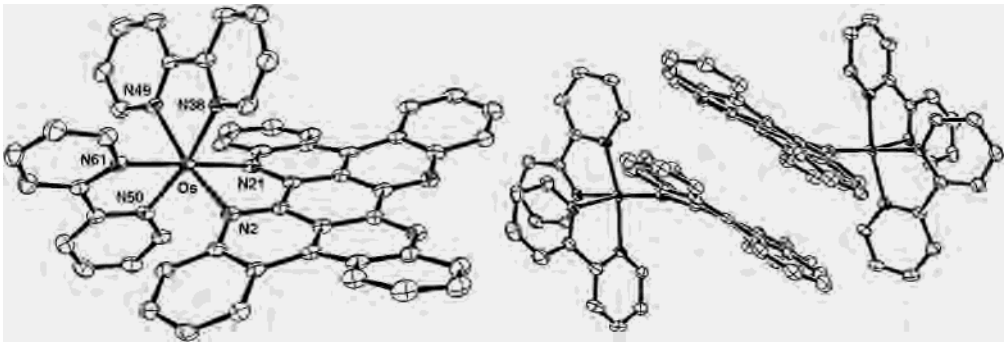


**Figure 5.** Left: ORTEP view of **4**, with partial atom labeling. Right: Crystal packing of **4**, exhibiting formation of a heterochiral dimer by complementary $\pi$-stacking from the exposed face of the dibenzoeilatin ligand.

discernment of the two faces of the dibenzoeilatin ligand, as one side is shielded while the other is extremely exposed. This tilting, combined with the S curvature of the dibenzoeilatin surface, ultimately determines the crystal packing (Figure 5, right): **4** arranges as discrete heterochiral dimers held together by complementary $\pi$-stacking interactions via the dibenzoeilatin ligand from its exposed face. The complementarity stems from the curvature of the dibenzoeilatin ligand, as efficient stacking can occur only when the two complex molecules are perfectly aligned in the dimer. The Os···Os distance in the dimer is 9.26 Å, as observed for **2**.[14] This distance is extremely short and implies extensive interpenetration of the two dibenzoeilatin surfaces.

**Table 1.** Selected Bond Lengths (Å) and Angles (deg) for **4**

| | |
|---|---|
| Os−N(2) | 2.072(3) |
| Os−N(21) | 2.076(3) |
| Os−N(38) | 2.084(3) |
| Os−N(49) | 2.096(3) |
| Os−N(50) | 2.062(3) |
| Os−N(61) | 2.067(3) |
| N(2)−Os−N(21) | 77.42(13) |
| N(38)−Os−N(49) | 78.18(13) |
| N(50)−Os−N(61) | 78.25(13) |

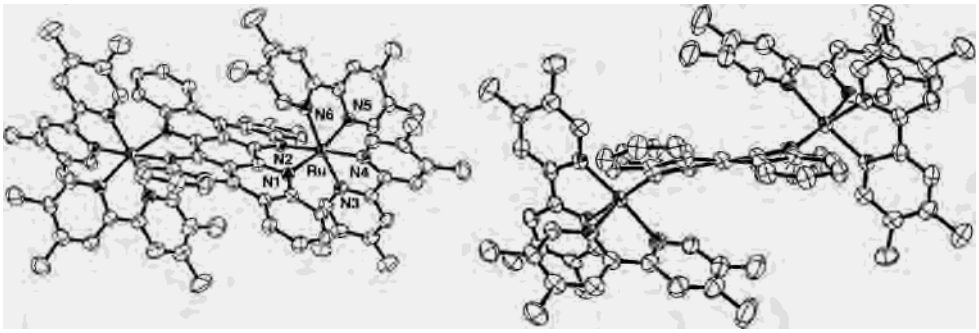


**Figure 6.** Left: ORTEP view of *meso*-**6**, with partial atom labeling. Right: ORTEP side view of *meso*-**6**.

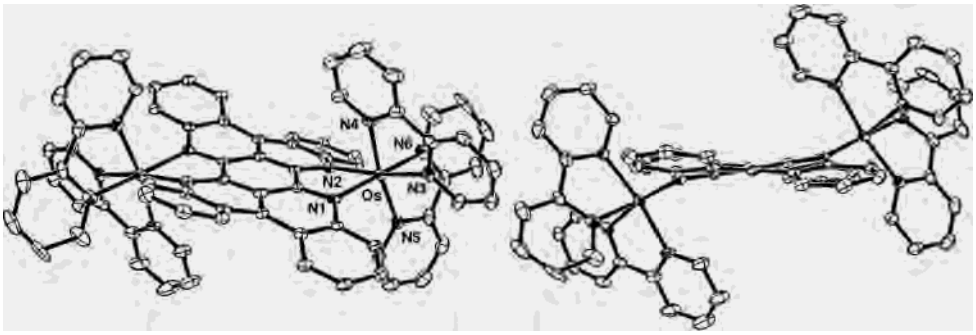


**Figure 7.** Left: ORTEP view of *meso*-**7**, with partial atom labeling. Right: ORTEP side view of *meso*-**7**.

**Table 2.** Selected Bond Lengths (Å) and Angles (deg) for *meso*-**6** and *meso*-**7**

| | *meso*-**6** | *meso*-**7** |
|---|---|---|
| M−N(1) | 2.082(4) | 2.087(3) |
| M−N(2) | 2.055(4) | 2.069(3) |
| M−N(3) | 2.080(4) | 2.087(3) |
| M−N(4) | 2.070(4) | 2.093(3) |
| M−N(5) | 2.056(4) | 2.055(3) |
| M−N(6) | 2.037(4) | 2.063(4) |
| N(1)−M−N(2) | 78.89(14) | 77.66(13) |
| N(3)−M−N(4) | 78.28(16) | 78.17(14) |
| N(5)−M−N(6) | 78.60(16) | 78.58(14) |

Crystallization of the dinuclear complexes proved to be challenging, as X-ray quality crystals of such complexes are notoriously difficult to obtain. Nevertheless, suitable crystals of **6** and **7** were obtained by changing the counterion and crystallization solvent: **6** was crystallized as the $OH^-$ salt from $CH_3OH/H_2O$, and **7** was crystallized as the $Cl^-$ salt from $CH_3CN/CH_3OH/H_2O$. Both complexes crystallized in a triclinic $P\bar{1}$ unit cell, and they represent the corresponding *meso* diastereoisomers. The perspective views (ORTEP) of the dinuclear complexes *meso*-**6** and *meso*-**7** with partial atom numbering are shown in Figures 6 and 7, respectively; selected bond distances and angles are given in Table 2. The asymmetric unit of *meso*-**6** contains half a complex molecule (located on a center of inversion) and, in addition to the two hydroxyl counterions, at least 10 molecules of partly disordered molecules of water (the poor quality of the crystals, and thus of the diffraction data, did not allow us to locate reliably all the hydrogen atoms of the located solvent). The asymmetric unit of *meso*-**7** contains one complex molecule, four chloride counterions, and crystallization solvent (14 molecules of water, and traces of acetonitrile). Both structures exhibit the same tilting of the metal centers with respect to the idealized equatorial plane of the $MN_6$ octahedron that was observed in the structures of the mononuclear complexes **2** and **4**. The tilting positions the two metal atoms on opposite sides of bridging ligand, so that they are relatively remote from one another. The M−N bond distances are comparable to those reported for Ru/Os polypyridyl complexes.[29,30]

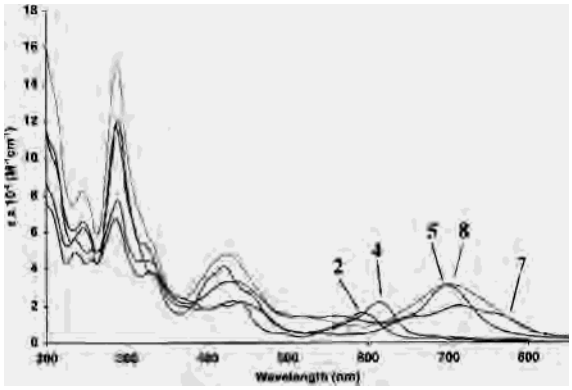


**Figure 8.** Absorption spectra of the mononuclear complexes **2** and **4**, and of the dinuclear complexes **5**, **7**, and **8**, recorded in acetonitrile.

**Absorption Spectra.** The UV−vis spectra of all complexes were recorded in acetonitrile; absorption spectra are illustrated in Figures 8 and 9, and absorption data listing energy maxima and absorption coefficients are summarized in Table 3. Due to the substantial insolubility of dibenzoeilatin, its absorption spectrum was not measured. The assignments of the absorption bands were based on the well-documented optical transitions of $[Ru(bpy)_3]^{2+}$ and $[Os(bpy)_3]^{2+}$,[1a,8b,31] and were supported by electrochemical measurements (vide infra). The absorption spectra of the

(30) Breu, J.; Stoll, A. J. *Acta Crystallogr., Sect. C* **1996**, *52*, 1174.
(31) Börje, A.; Köthe, O.; Juris, A. *J. Chem. Soc., Dalton Trans.* **2002**, 843.

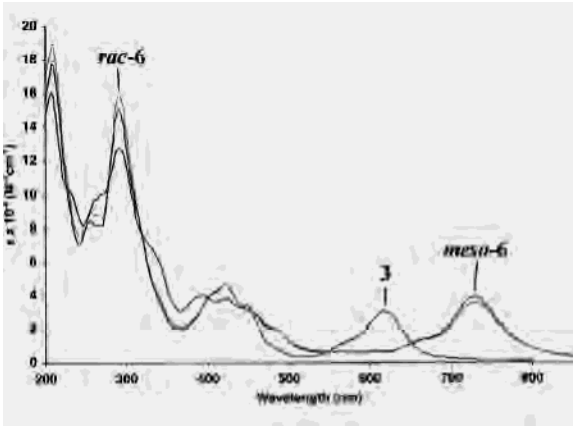


**Figure 9.** Absorption spectra of the mononuclear complex **3**, and of the two diastereoisomers of **6**, *meso* and *rac*.

**Table 3.** Absorption Data[a]

| complex | absorption maxima $\lambda_{max}$, nm ($\epsilon \times 10^{-4}$ $M^{-1}$ $cm^{-1}$) |
|---|---|
| $[Ru(bpy)_3]^{2+}$ [b] | 250(2.5), 285(8.7), 323sh, 345sh, 452(1.4) |
| $[Os(bpy)_3]^{2+}$ [c] | 290(7.8), 436(1.1), 478(1.1), 579(0.3) |
| **2**[d] | 202sh, 236(4.9), 257(4.6), 286(6.8), 330(3.9), 375sh, 419(2.1), 441(2.4), 547sh, 594(1.5) |
| **3** | 207(11.1), 231sh, 266sh, 292(13.2), 333sh, 393(3.9), 422(3.8), 447(3.3), 571sh, 618(2.8) |
| **4** | 202sh, 236(5.6), 254sh, 257(5.1), 289(8.0), 323(4.6), 376sh, 433(2.3), 566sh, 615(2.2) |
| **5** | 208sh, 245(6.2), 287(9.2), 336sh, 400sh, 421(4.2), 452sh, 646sh, 699(2.9). |
| *meso*-**6** | 209(11.5), 255(8.4), 291(12.1), 405sh, 422(4.6), 450sh, 490sh, 670sh, 729(3.9) |
| *rac*-**6** | 208(11.5), 256(9.0), 291(12.6), 402sh, 422(4.6), 449sh, 481sh, 661sh, 729(3.6) |
| **7** | 208sh, 246(6.7), 290(10.7), 323sh, 426(3.2), 437(3.2), 510sh, 565sh, 664sh, 714(1.9), 771sh |
| **8** | 210sh, 245(8.2), 289(12.9), 324sh, 426(4.6), 518sh, 639sh, 700(3.0), 752sh |

[a] Recorded in acetonitrile. [b] From ref 1a. [c] From ref 8b and 31. [d] From ref 14.

mononuclear complexes exhibit intense absorption bands in the UV region (200−350 nm), assigned to ligand-centered (LC) $\pi \rightarrow \pi^*$ transitions of the peripheral ligands. In the visible region, the band centered around 420 nm is assigned to dibenzoeilatin-centered $\pi \rightarrow \pi^*$ transitions, overlapping with $d_\pi(M) \rightarrow \pi^*(N-N)$ metal-to-ligand charge transfer (MLCT) transitions. In addition, the spectra exhibit a broad low-lying absorption band centered around 600 nm, assigned to $d_\pi(M) \rightarrow \pi^*$(dbneil) MLCT transitions. The combination of absorptions at 600 and 420 nm renders these complexes their dark green color.

Upon coordination of a second metal fragment, a clear color change is observed. While the all-ruthenium complexes **5** and **6** exhibit an intense yellow-green color, the dinuclear osmium-containing complexes **7** and **8** exhibit a dark brown color. These color changes result from shifting of the $d_\pi(M) \rightarrow \pi^*$(dbneil) MLCT transition to longer wavelengths: 700 nm for **5** and **8**, 714 nm for **7**, and 730 nm for **6**. The major low-energy MLCT band of the homodinuclear osmium complex **7** is accompanied by two shoulders at ca. 770 and 660 nm, whereas the low-energy MLCT band of the heterodinuclear complex **8** is very broad but does not exhibit any splitting pattern. The tailing of the absorption to the near-IR region observed for the dinuclear Os-containing

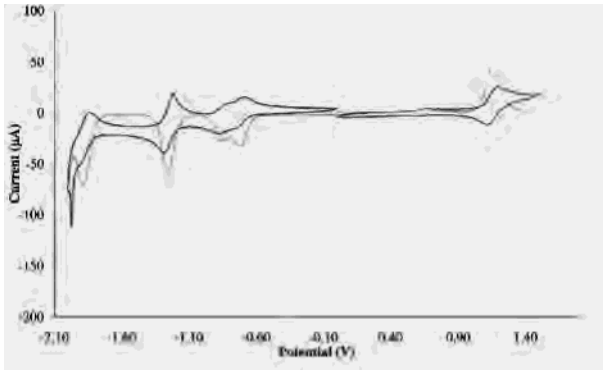


**Figure 10.** Cyclic and square wave voltammograms of the mononuclear complex **2**, vs $Ag/AgNO_3$.

complexes is attributable to spin-forbidden $^3$MLCT transitions, which gain intensity due to enhanced spin−orbit coupling induced by the heavy Os centers.[32] The dinuclear complexes exhibit higher extinction coefficients than the corresponding monometallic species, as expected by the addition of a second chromophoric $M(N-N)_2$ unit, and also a broadened absorption around 420 nm, spanning from 350 to 500 nm. All other features of the absorption spectra of the dinuclear complexes are similar to those of their mononuclear counterparts. Only slight differences were observed between the absorption spectra of *meso*-**6** and *rac*-**6**; we assume that this holds also for all the other dinuclear complexes, which were characterized as the diastereoisomeric mixtures.

**Electrochemistry.** The redox behavior of all the complexes was studied in acetonitrile solution, employing cyclic and square wave voltammetry techniques. $E_{1/2}$ values of successive closely spaced reduction processes were determined using the peak potential value ($E_p$) from the square wave voltammograms. The results are collected in Table 4, together with the data of $[Ru(bpy)_3]^{2+}$ and $[Os(bpy)_3]^{2+}$ obtained under the same conditions.[1a,33] Both *meso*-**6** and *rac*-**6** exhibited identical redox behavior;, therefore, the results are reported for the mixture of the two diastereoisomers.

The mononuclear complexes display a single reversible metal-centered oxidation ($M^{II/III}$). The oxidation potential of the metal center in **2** is anodically shifted with respect to that of $[Ru(bpy)_3]^{2+}$ (1.46 V vs 1.28 V vs SCE, respectively) (Figure 10). Replacement of the bpy ligands with tmbpy results in a 0.15 V cathodic shift in the oxidation potential of the Ru center, the process occurring at 1.31 V versus SCE for **3**. Analogously, the oxidation potential of the Os center in **4** is anodically shifted with respect to that of $[Os(bpy)_3]^{2+}$ (1.09 V vs 0.81 V vs SCE). The three mononuclear complexes exhibit several successive one-electron ligand-centered reductions. The first reversible one-electron reduction wave, appearing at around −0.5 V, is split into two small waves, as observed previously for mononuclear eilatin complexes.[34] The second quasireversible one-electron reduc-

(32) Kober, E. M.; Caspar, J. V.; Sullivan, B. P.; Meyer, T. J. *Inorg. Chem.* **1988**, *27*, 4587.
(33) Jandrasics, E. Z.; Keene, F. R. *J. Chem. Soc., Dalton Trans.* **1997**, 153.

**Table 4.** Half-Wave Potentials for the Oxidation and the Reduction of the Complexes[a]

| complex | $Ru^{II/III}$ | | $Os^{II/III}$ | | $E_{red1}$ | | $E_{red2}$ | $E_{red3}$ | $E_{red4}$ |
|---|---|---|---|---|---|---|---|---|---|
| $[Ru(bpy)_3]^{2+}$ [b] | 1.28 | | | | −1.33 | | −1.53 | −1.78 | |
| $[Os(bpy)_3]^{2+}$ [c] | | | 0.81 | | −1.29 | | −1.46 | −1.79 | |
| **2** | 1.46(80) | | | | −0.41(50) | −0.56(50) | −0.95(60) | −1.58[d] | |
| **3** | 1.31(90) | | | | −0.50(60) | −0.61(50) | −1.00(60) | −1.73(90) | |
| **4** | | | 1.09(90) | | −0.42(50) | −0.54(50) | −0.89[d] | −1.46[d,e] | −1.56[d,e] |
| **5** | 1.49(80) | 1.65(80) | | | −0.16(60) | | −0.57(60) | −1.30[d,e] | −1.51[d,e] |
| **6** | 1.34(90) | 1.52(90) | | | −0.23(60) | | −0.64(60) | −1.37(90) | |
| **7** | | | 1.07(60) | 1.32(60) | −0.21(60) | | −0.55(60) | −1.18[d,e] | −1.35[d,e] |
| **8** | 1.63(90) | | 1.14(60) | | −0.18(60) | | −0.55(60) | −1.26[d,e] | −1.45[d,e] |

[a] Potentials are given vs SCE in acetonitrile, with 0.1 M $Bu_4NPF_6$ as supporting electrolyte, measured at room temperature with scan rate of 0.1 V/s, $\Delta E_p$ values in mV given in parentheses. [b] From ref 1a. [c] From ref 33. [d] Values determined from square wave voltammetry. [e] Unresolved processes.

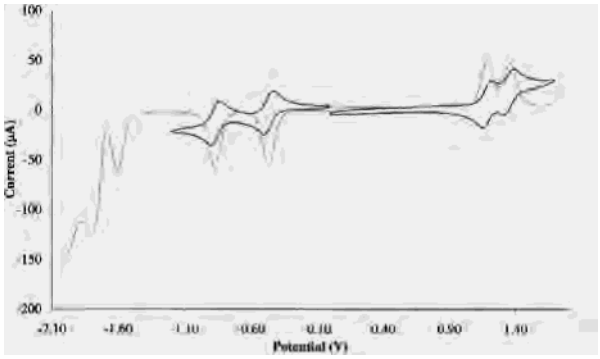


**Figure 11.** Cyclic and square wave voltammograms of the dinuclear complex **5**, vs $Ag/AgNO_3$.

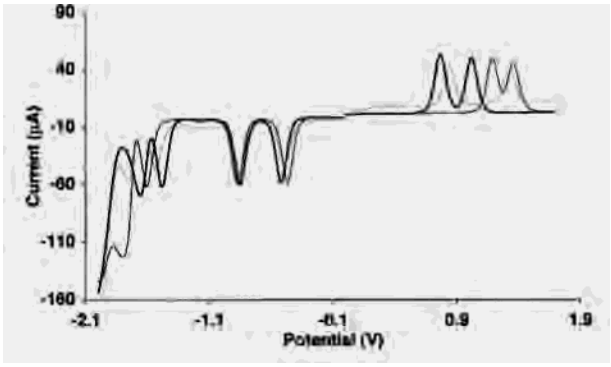


**Figure 12.** Square wave voltammograms of the homodinuclear complexes **5** (black line) and **7** (bold black line), and of the heterodinuclear complex **8** (gray line), vs $Ag/AgNO_3$.

tion wave, appearing at around −0.9 V, is complicated by desorption peaks, and is well-resolved only for **3**. The first two reduction processes occur at significantly anodically shifted potentials compared to $[Ru(bpy)_3]^{2+}$ and $[Os(bpy)_3]^{2+}$ and are therefore attributed to two consecutive reductions of the highly conjugated dibenzoeilatin ligand. Additional reduction waves attributed to reduction of the peripheral bpy and tmbpy ligands appear at further cathodic potentials but are ill-resolved due to desorption peaks.

The homodinuclear complexes exhibit two reversible, well-resolved metal-centered oxidations. The first oxidation process occurs at potentials comparable to the mononuclear complexes. The second oxidation process is anodically shifted, the difference between the two oxidation processes being 0.16 V for **5**, 0.18 V for **6**, and 0.25 V for **7** (Figure 11 and 12). The heterodinuclear complex **8** also exhibits two reversible metal-centered oxidations at 1.14 and 1.63 V versus SCE, corresponding to the oxidation of the Os and Ru centers, respectively. All dinuclear complexes exhibit two successive, reversible, one-electron reductions of the bridging dibenzoeilatin ligand, occurring at −0.16 and −0.57 V versus SCE for **5**, at −0.23 and −0.64 V versus SCE for **6**, at −0.21 and −0.54 V versus SCE for **7**, and at −0.18 and −0.55 V versus SCE for **8**, respectively. The first reduction process is not split and is substantially anodically shifted (ca. 0.3 V) compared to the first (split) reduction process of the corresponding mononuclear complex. Subsequent reduction waves attributed to the reduction of the peripheral bpy and tmbpy ligands are also anodically shifted compared to the mononuclear counterparts, but to a lesser extent, and are unresolved due to desorption peaks.

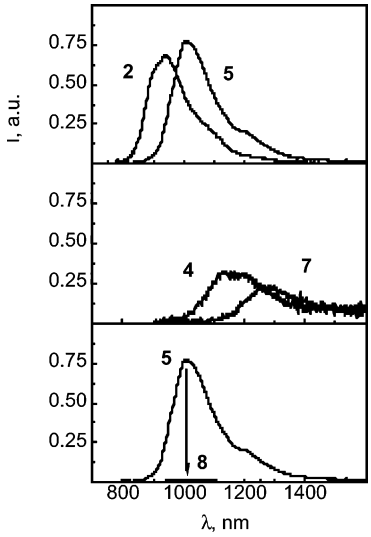


**Figure 13.** Luminescence spectra of isoabsorbing solutions ($\lambda_{exc}$ = 440 nm) of the indicated complexes.

**Luminescence.** The emission spectra of the complexes were recorded at room temperature in argon-purged acetonitrile solutions. Representative spectra are illustrated in Figure 13; emission band maxima ($\lambda_{max}$), emission quantum yield ($\Phi$), and lifetime ($\tau$) values are collected in Table 5, together with known data of $[Ru(bpy)_3]^{2+}$ and $[Os(bpy)_3]^{2+}$. The values for **6** are reported for the diastereoisomeric mixture. For all the complexes, the excitation wavelength was 440 nm for the luminescence spectra, and 407 nm for lifetimes; this is expected to lead to the population of singlet levels of dibenzoeilatin origin, with final population of the lowest available $^3$MLCT levels either of Ru- or Os-based

(34) Gut, D.; Goldberg, I.; Kol, M. *Inorg. Chem.* **2003**, *42*, 3483.

**Table 5.** Luminescence and Photophysical Properties[a]

| complex | $\lambda_{max}$[b] (nm) | $\Phi$[c] | $\tau$ (ns) | $k_r \times 10^{-4}$ [c] ($s^{-1}$) | $k_{nr} \times 10^{-7}$ [c] ($s^{-1}$) |
|---|---|---|---|---|---|
| $[Ru(bpy)_3]^{2+}$ | 626 | 0.062 | 900 | 6.9 | 10.0 |
| $[Os(bpy)_3]^{2+}$ | 740 | $5.0 \times 10^{-3}$ | 49 | 10.2 | 2.0 |
| **2** | 952 | $4.8 \times 10^{-4}$ | 18 | 2.6 | 5.5 |
| **3** | 1010 | $2.6 \times 10^{-4}$ | 15 | 1.8 | 6.8 |
| **4** | 1132 | $6.1 \times 10^{-5}$ | 4 | 1.5 | 25.0 |
| **5** | 1028 | $5.6 \times 10^{-4}$ | 30 | 1.9 | 3.4 |
| **6** | 1086 | $2.3 \times 10^{-4}$ | 14 | 1.7 | 7.4 |
| **7** | 1270 | $3.0 \times 10^{-5}$ | 2 | 1.5 | 50.0 |
| **8** | 1032 | | | | |

[a] At room temperature in argon-purged acetonitrile. All the complexes were measured as the hexafluorophosphate salts; $\lambda_{exc} = 440$ nm (luminescence spectra) or 407 nm (luminescence lifetimes), see text. [b] From corrected spectra, see text. [c] From $k_r = \Phi/\tau$ and $k_{nr} = 1/\tau - k_r$.

origin, as occurs for the prototypical complexes $[Ru(bpy)_3]^{2+}$ and $[Os(bpy)_3]^{2+}$.[21b,22]

For Ru(II) and Os(II) polypyridyl complexes, a correlation exists between the electrochemical and spectroscopic data.[1a,35] As complexes **2**−**8** exhibit both low-lying MLCT transitions in the absorption spectra and anodically shifted reduction potentials of the dibenzoeilatin ligand, the luminescent $^3$MLCT levels of these complexes are expected to be substantially red-shifted compared to $[Ru(bpy)_3]^{2+}$.[1a,22] This is indeed observed, the emission maxima occurring at 952 nm for **2**, 1010 nm for **3**, and 1132 nm for **4**. The homodinuclear complexes exhibit emissions that are even further red-shifted, occurring at 1028 nm for **5**, 1086 nm for **6**, and 1270 nm for **7**. Interestingly, the heterodinuclear complex **8** features luminescence emission only from the Ru-based unit, occurring at 1032 nm, the intensity of which is depressed to less than 1% of that exhibited by the homodinuclear complex **5** (Figure 13, bottom).

## Discussion

The synthesis of mononuclear complexes of a bridging ligand is often accompanied by the formation of dinuclear species.[36] Formation of such byproducts is usually minimized by employing relatively mild reaction conditions and by using an excess of the bridging ligand. In the case of dibenzoeilatin, we found that changing the molar ratio of dibenzoeilatin to metal precursor had no beneficial effect, and a substantial amount of the dinuclear species was always obtained. This is in sharp contrast to the high selectivity for the formation of mononuclear complexes exhibited by the related eilatin ligand, whose two coordination sites have different steric bulk.[37] Formation of dinuclear eilatin complexes requires relatively harsh conditions, attributed to a higher energetic barrier, as the ligand distorts from planarity upon coordination of a metal fragment to its sterically hindered biq-type "tail".[34] In contrast, the intrinsic distortion of the dibenzoeilatin bridging ligand renders it preorganized for the second complexation event. The relatively harsh reaction conditions required for the synthesis of the mononuclear dibenzoeilatin complexes are due to its sterically hindered biq-type coordination sites and its profound insolubility. However, once the first complexation occurs, the second complexation follows quite rapidly, as the mononuclear complex is very soluble in ethylene glycol, and its remaining coordination site is preorganized for complexation.

In the solid state, the mononuclear dibenzoeilatin complexes form discrete heterochiral dimers held together by complementary $\pi-\pi$ stacking interactions via the dibenzoeilatin moiety. We have previously shown that there is a correlation between the metal-to-metal separation observed in the solid-state dimer and the magnitude of the dimerization constant measured in solution.[14,15] The metal-to-metal distances in both crystal structures of **2** and **4** are identical. The X-ray data correlate well with the $^1$H NMR data, as **2** and **4** have, within experimental error, the same dimerization constant ($K_d \approx 720$ $M^{-1}$ at ca. 297 K), which is ca. 2.5 times higher than that measured for related eilatin complexes.[14,15] The identical metal-to-metal distance in **2** and **4** may imply that these complexes stack with maximum possible overlap.

The tilt conformation observed in the mononuclear complexes is also maintained in the dinuclear complexes, while the S curvature of the dibenzoeilatin ligand dictates the direction of the tilting. Indeed, in both crystal structures of *meso*-**6** and *meso*-**7**, each metal fragment points toward a different direction, a situation that does not permit any spatial communication between them; i.e., the chirality and bulk of ligands around a specific metal center are not reflected at the other metal center. According to $^1$H NMR spectrum of crude **6**, and supported by the spectra of all the other bimetallic complexes, the dinuclear complexes form as 1:1 mixtures of the *meso* and *rac* isomers. We propose that the lack of diastereomeric preference in their formation results from this lack of communication (this is in contrast to the 3:1 preference in favor of the *meso* isomer observed in formation of dinuclear eilatin complexes[34]). On the NMR time scale, we observe a single, simple set of peaks, which would suggest that the dinuclear complexes undergo a fast "wagging" motion, i.e., that dibenzoeilatin flips and the two metal fragments move up and down. This motion renders the *meso* and *rac* complexes their time-averaged symmetries of $C_{2h}$ and $D_2$, respectively.

The absorption spectra of the mononuclear complexes **2**, **3**, and **4** all exhibit the same general features, with the distinction being the wavelength of the lowest-energy MLCT transition, appearing at 594 nm for **2**, at 618 nm for **3**, and at 615 nm for **4**. The lower energy of the $d_\pi$(Ru) → $\pi^*$(dbneil) MLCT transition in **3** relative to **2** results from the higher lying $d_\pi$(Ru) orbital, due to the electron-donating methyl groups on the peripheral bpy ligands. A similar red-shifting of the $d_\pi$(M) → $\pi^*$(dbneil) MLCT transition is observed on going from Ru to Os (**4** relative to **2**), as expected of the higher-lying $d_\pi$(Os) orbitals.

(35) Vlcek, A. A.; Dodsworth, E. S.; Pietro, W. J.; Lever, A. B. P. *Inorg. Chem.* **1995**, *34*, 1906.

(36) There are several examples in the literature where selectivity was achieved due to inequivalence of the two binding sites of the ligand; see for example: (a) Thummel, R. P.; Williamson, D.; Hery, C. *Inorg. Chem.* **1993**, *32*, 1587. (b) Ward, M. D. *J. Chem. Soc., Dalton Trans.* **1993**, 1321. (c) Rau, S.; Ruben, M.; Büttner, T.; Temme, C.; Dautz, S.; Görls, H.; Rudolph, M.; Walther, D.; Brodkorb, A.; Duati, M.; O'Connor, C.; Vos, J. G. *J. Chem. Soc., Dalton Trans.* **2000**, 3649. (d) Reference 34.

(37) Rudi, A.; Kashman, Y.; Gut, D.; Lellouche, F.; Kol, M. *Chem. Commun.* **1997**, 17.

The lowest-energy MLCT transition of the dinuclear complexes exhibits significant red shifts (ca. 100 nm) compared to the corresponding mononuclear complexes, due to stabilization of the dibenzoeilatin-centered $\pi^*$ orbital. The intensity of the lowest MLCT transition in the dinuclear complexes is ca. twice as high as that of the analogous mononuclear species, as expected upon the addition of a second chromophoric $[M(N-N)_2]^{2+}$ unit. Furthermore, as observed for the mononuclear complexes, addition of the methyl substituents onto the peripheral bpy ligands, or changing the metal center from Ru to Os, causes a red-shifting of the $d_\pi(M) \rightarrow \pi^*$(dbneil) MLCT band. The other bands of the absorption spectra of the dinuclear complexes are not affected substantially with respect to those of the mononuclear complexes, the most pronounced difference being the higher extinction coefficient for the high-energy LC transitions ($\pi \rightarrow \pi^*$) attributed to the increase in the number of peripheral N−N ligands. All the absorption bands in the spectrum of the heterodinuclear complex **8** appear broad and lacking in fine detail in comparison to those of the homodinuclear complexes. This may be attributed to overlapping of slightly different bands resulting from the two different metals. The diastereoisomers of **6** exhibit similar, though not identical, spectra, as slight differences in $\lambda_{max}$ and extinction coefficients are observed (repeated experiments confirmed these differences). While the effect of diastereoisomerism on physical properties in related systems is still under debate,[38,39] our findings show that for the dibenzoeilatin complexes stereochemistry has only slight influence on the electronic transitions.

All the mononuclear complexes exhibit metal-centered oxidation processes that are anodically shifted with respect to the appropriate $[M(bpy)_3]^{2+}$ analogues, since dibenzoeilatin is a strong $\pi$-acceptor ligand that stabilizes the $d_\pi(M)$ orbitals. Addition of electron-donating methyl groups onto the peripheral bpy ligands causes destabilization of the metal-centered orbitals, leading to a cathodic shift of the oxidation process on going from **2** to **3**. The higher lying metal-centered orbitals in Os lead to more facile oxidation of **4** compared to that of **2**. Consistent with the low-lying $\pi^*$ orbital of dibenzoeilatin, the bridging ligand-based reductions occur at substantially anodically shifted potentials compared to bpy ligands. The splitting of the first reduction wave of the mononuclear dibenzoeilatin complexes can be explained by their strong tendency to form discrete dimers in solution held together by strong, complementary $\pi$-stacking interactions, so that the species undergoing the first reduction process is actually a dimer.[34,40]

**Table 6.** Calculated $k_{com}$ Values of the Homodinuclear Complexes[a]

| complex | $E_{ox1}$ | $E_{ox2}$ | $\Delta E$ | $k_{com}$ |
|---|---|---|---|---|
| **5** | 1.49 | 1.65 | 0.16 | $0.5 \times 10^3$ |
| **6** | 1.34 | 1.52 | 0.18 | $1.1 \times 10^3$ |
| **7** | 1.07 | 1.32 | 0.25 | $1.7 \times 10^4$ |

[a] Calculated using $T = 298$ K.

Coordination of a second metal fragment further lowers the energy of the $\pi^*$(dbneil) orbital, leading to a substantial anodic shift of the bridging ligand's reduction potentials. The first reduction process of the bimetallic species is not split, consistent with NMR data and X-ray data that clearly show its inability to $\pi$-stack. The homodinuclear complexes exhibit two distinct metal-centered oxidation potentials, even though the two metal centers are chemically equivalent. The separation between the half-wave potentials of the two oxidation processes ($\Delta E = 0.16$ V for **5**, 0.18 V for **6**, and 0.25 V for **7**) is a measure of the extent of electronic coupling between them.[41] The metal-to-metal distance in the dinuclear complexes (ca. 7.9 Å), combined with their relative orientation, is unlikely to permit through-space coupling. The metal−metal interaction can be explained on the basis of superexchange theory,[7] where the overlap between the metal orbitals is mediated by the orbitals of the bridging ligand. The extent of interaction depends on the energy gap between the metal-centered $d_\pi$ orbital and the HOMO/LUMO of the bridging ligand. Compound **7** exhibits a larger splitting of the two oxidation waves compared to **5**. This is consistent with an electron-transfer mechanism, as opposed to a hole-transfer mechanism, as the higher-lying $d_\pi$ orbitals of Os undergo extensive mixing with the $\pi^*$ orbital of the dibenzoeilatin ligand because the energy gap between them is smaller.[7c] The sequential one-electron oxidations produce mixed-valence species, the stability of which can be expressed in terms of the comproportionation constant, $k_{com}$:[39d,42]

$$k_{com} = \exp(nF\Delta E/RT) \qquad (1)$$

where $\Delta E$ is the difference between the two oxidation potentials in volts. The $k_{com}$ values for the dinuclear complexes presented in Table 6 suggest moderate electronic coupling between the metal centers.

The heterodinuclear complex **8** also exhibits two well-resolved oxidation processes: The first oxidation process, corresponding to the $Os^{II/III}$ couple, is anodically shifted with respect to the first oxidation process observed for **7**, whereas the second oxidation process, corresponding to the $Ru^{II/III}$ couple, is slightly cathodically shifted with respect to the second oxidation process in **5**. Both observations reflect the greater electron withdrawing capabilities of Ru and its diminished tendency to back-donate relative to Os.

The luminescence features recorded at room temperature are consistent with a wealth of previous observa-

(38) For the lack of influence, see for example: (a) Ernst, S. D.; Kaim, W. *Inorg. Chem.* **1989**, *28*, 1520. (b) Denti, G.; Campagna, S.; Serroni, S.; Ciano, M.; Balzani, V. *J. Am. Chem. Soc.* **1992**, *114*, 2944. (c) Reference 8e.

(39) For the influence, see for example: (a) Kelso, L. S.; Reitsma, D. A.; Keene, F. R. *Inorg. Chem.* **1996**, *35*, 5144. (b) Reference 10c. (c) Keene, F. R. *Chem. Soc. Rev.* **1998**, *27*, 185 and references therein. (d) Paul, P.; Tyagi, B.; Bilakhiya, A. K.; Dastidar, P.; Suresh, E. *Inorg. Chem.* **2000**, *39*, 14. (e) Richardson, C.; Steel, P. J.; D'Alessandro. D. M.; Junk, P. C.; Keene, F. R. *J. Chem. Soc., Dalton Trans.* **2002**, 2775.

(40) Gut, D. Unpublished results.

(41) Demadis, K. D.; Hartshorn, C. M.; Meyer, T. J. *Chem. Rev.* **2001**, *101*, 2655 and references therein.

(42) (a) Robin, M. B.; Day, P. *Adv. Inorg. Chem. Radiochem.* **1967**, *10*, 247. (b) Creutz, C. *Prog. Inorg. Chem.* **1983**, *30*, 1. (c) Richardson, D. E.; Taube, H. *Coord. Chem. Rev.* **1984**, *60*, 107. (d) Richter, M. M.; Brewer, K. J. *Inorg. Chem.* **1993**, *32*, 2827.

tions.[1,22,39,41,43−49] On passing from the mononuclear Ru-based complex **2** to its dinuclear counterpart **5**, a red shift is observed in the emission band maximum (from 952 to 1028 nm, respectively). This is consistent with the stabilization of the $\pi^*$ orbital of the dibenzoeilatin ligand (which is involved in the $^3$MLCT emission) by the coordination of a second metal center, as observed both in the absorption spectra and the electrochemical measurements. The dinuclear complex **5** exhibits slightly higher luminescence intensity and longer lifetime with respect to the mononuclear complex **2**. This might be explained by the stabilization of the emissive level of **5** compared to **2**, resulting in more difficult thermal access of the higher-lying $^3$MC levels from which fast radiationless processes occur, as has been demonstrated for Ru−polypyridyl complexes.[43] However, stabilization of the emitting level is also predicted to lead to some enhancement of nonradiative transitions, on the basis of the energy-gap law.[43−45] This might explain the behavior exhibited by the mononuclear complex **3** and its dinuclear counterpart **6**, where stabilization of the emissive levels (from 1010 to 1086 nm, respectively) only slightly affects the luminescence quantum yield and lifetime (see Table 5). In this case, the effect due to the energy-gap law might counterbalance the effect due to the thermal access of the $^3$MC levels, and the radiationless paths governed by the energy-gap law could be more effective for **6** (emission maximum 1086 nm) compared to **5** (emission maximum 1028 nm).[43−45] The Os-based complexes exhibit a clear-cut trend; on passing from the mononuclear complex **4** to its dinuclear counterpart **7**, both the luminescence intensity and lifetime are reduced. It is known that for Os−polypyridyl complexes no $^3$MC levels are thermally accessible from the $^3$MLCT luminescent levels.[22] The behavior exhibited by **4** and **7** is therefore well explained by the expected effect from the energy-gap law.[43−45]

The heterodinuclear complex **8** exhibits only Ru-based emission at 1032 nm, with an intensity ($I$) that is depressed to less than 1% of that exhibited by the model homodinuclear complex **5** ($I_0$). The rate constant $k_q$ of the quenching observed for the Ru-based emission of **8** can be estimated using eqs 2 and 3, where $\tau_0 = 27$ ns for the model complex **5**.[46]

$$k_q = \frac{1}{\tau} - \frac{1}{\tau_0} \quad (2)$$

$$k_q = \frac{1}{\tau_0}\left(\frac{I_0}{I} - 1\right) \quad (3)$$

Thus, for **8**, a quenching rate constant of $k_q \geq 3 \times 10^9$ s$^{-1}$ is evaluated. For heterodinuclear complexes containing Ru- and Os-based polypyridine units, quenching of the luminescent, higher-lying Ru-based $^3$MLCT level by energy transfer, leading to sensitization of the lower-lying Os-based $^3$MLCT level, is a well-documented event.[1d,46−49] For the case of **8**, the driving force for the occurrence of such an intramolecular *Ru → Os energy transfer process is ca. 0.25 eV as evaluated from the onset of luminescence bands of **5** and **7** (1.38 and 1.13 eV, respectively). However, no *Ru → Os energy transfer takes place because no Os-based luminescence (neither intrinsic nor from sensitization) is observed for this complex, in contrast with what is observed in most of the Ru/Os heterometallic polypyridyl complexes investigated thus far.[1d,46−49] The energy content of the Ru-based $^3$MLCT level (1.38 eV), the oxidation potential of the Os center (1.14 V), and the reduction potential of the bridging dibenzoeilatin ligand (−0.18 V) suggest that there is a slightly favorable driving force ($\Delta G = -0.06$ eV) for the occurrence of reductive quenching by *Ru ← Os electron transfer for complex **8**. This step would result in no Os-based emission, as found experimentally.

## Conclusions

The dibenzoeilatin ligand features a unique combination of two identical biq-type coordination sites, a large fused aromatic surface, and an innate distortion from planarity. This combination leads to difficult formation of mononuclear species and, in contrast, facile formation of dinuclear species, as well as a strong tendency to aggregate by complementary $\pi$-stacking interactions. The low-energy dibenzoeilatin-centered $\pi^*$ orbital is responsible for the interesting absorption and electrochemical behavior and near-IR emission properties, a rare feature in Ru(II) and Os(II) polypyridyl complexes. Although the distortion of the dibenzoeilatin ligand directs the two metal centers away from each other, the electronic communication between them is substantial, as evident from the electrochemical measurements. Further studies aimed at revealing the parameters affecting this communication are under way.

**Acknowledgment.** This research was supported by the Israel Science Foundation founded by the Israel Academy of Sciences and Humanities, and by the FIRB project RBNE019H9K "Molecular Manipulation for Nanometric Devices" by MIUR. We thank Dr. Dalia Gut for valuable discussions and Mrs. Dvora Reshef for technical assistance.

**Supporting Information Available:** X-ray crystallographic files in CIF format for the structure determinations of complexes **4**, *meso*-**6**, and *meso*-**7**. This material is available free of charge via the Internet at http://pubs.acs.org.

IC0354062

(43) (a) Hammarström, L.; Barigelletti, F.; Flamigni, L.; Indelli, M. T.; Armaroli, N.; Calogero, G.; Guardigli, M.; Sour, A.; Collin, J. P.; Sauvage, J. P. *J. Phys. Chem. A* **1997**, *101*, 9061. (b) Treadway, J. A.; Loeb, B.; Lopez, R.; Anderson, P. A.; Keene, F. R.; Meyer, T. J. *Inorg. Chem.* **1996**, *35*, 2242. (c) Matacangay, A.; Zheng, G. Y.; Rillema, D. P.; Jackman, D. C.; Merkert, J. W. *Inorg. Chem.* **1996**, *35*, 6823.
(44) Englman, R.; Jortner, J. *Mol. Phys.* **1970**, *18*, 145.
(45) Caspar, J. V.; Kober, E. M.; Sullivan, B. P.; Meyer, T. J. *J. Am. Chem. Soc.* **1982**, *104*, 630.
(46) Barigelletti, F.; Flamigni, L.; Balzani, V.; Collin, J.-P.; Sauvage, J.-P.; Sour, A.; Constable, E. C.; Cargill-Thompson, A. M. W. *J. Am. Chem. Soc.* **1994**, *116*, 7692.
(47) Keene, F. R. *Coord. Chem. Rev.* **1997**, *166*, 121.
(48) De Cola, L.; Belser, P. *Coord. Chem. Rev.* **1998**, *177*, 301.
(49) Barigelletti, F.; Flamigni, L. *Chem. Soc. Rev.* **2000**, *29*, 1.